PERGAMON

Deep-Sea Research II 50 (2003) 167–195

DEEP-SEA RESEARCH
PART II

www.elsevier.com/locate/dsr2

Observations of a young Agulhas ring, Astrid, during MARE in March 2000

H.M. van Aken[a,*], A.K. van Veldhoven[a], C. Veth[a], W.P.M. de Ruijter[b], P.J. van Leeuwen[b], S.S. Drijfhout[c], C.P. Whittle[d], M. Rouault[d]

[a] *Royal Netherlands Institute for Sea Research (NIOZ), P.O. Box 59, 1790 AB Den Burg, Texel, Netherlands*
[b] *Institute for Marine and Atmospheric Research (IMAU), Utrecht University, P.O. Box 80005, 3508 TA Utrecht, Netherlands*
[c] *Royal Netherlands Meteorological Institute (KNMI), P.O. Box 201, 3730 AE De Bilt, Netherlands*
[d] *Department of Oceanography, University of Cape Town (UCT), 7700 Rondebosch, South Africa*

Received 7 January 2002; accepted 19 March 2002

Abstract

The MARE project studies the effects of inter-ocean exchange between the Indian and Atlantic Ocean, via Agulhas rings, on the Atlantic meridional overturning circulation. The field programme of MARE concentrates on the study of the decay and modification of a single Agulhas ring named Astrid, formed in January 2000. The ring was clearly visible in the analysis of satellite altimetry data, and surface drifters confirmed the anti-cyclonic rotation. During a detailed survey of this 2-month-old ring in March 2000, it appeared that the water mass properties of this ring only differed from the surrounding water above the 12°C isotherm. The observed fine-structure near its boundary suggested that exchange of water with its surroundings already had started. Observations with a lowered acoustic Doppler current profiler showed that the ring had a significant barotropic component, additional to the baroclinic flow around its warm centre. Meteorological observations indicated that during the summer survey the ring was losing heat to the atmosphere. This heat loss maintained convective mixing in the surface mixed layer. Compared to other reported rings, Astrid had a very large kinetic energy, a property probably characteristic for very young Agulhas rings. In other aspects Astrid did not differ strongly from the other rings, although Astrid was slightly larger than their typical 'average' size.

1. Introduction

The Agulhas Current flows southwestwards along the continental slope of South Africa as the western boundary current of the southwest Indian Ocean subtropical gyre. South of the Agulhas Bank, at the outer edge of the continental shelf, the Agulhas Current retroflects sharply, and continues eastwards as the Agulhas Return Current. At the Agulhas Retroflection the current regularly loops back upon itself, and large rings are shed from the main current and move into the South Atlantic Ocean (Gordon et al., 1987; Ou and De Ruijter, 1986). On average, five of these anti-cyclonic Agulhas rings are generated each year, although sometimes periods of over half a year occur without any ring shedding event (Goni et al., 1997; Schouten et al., 2000). Over 30 rings

*Corresponding author. Tel.: +31-222-369-416; fax: +31-222-319-674.
E-mail address: aken@nioz.nl (H.M. van Aken).

0967-0645/02/$ - see front matter
PII: S0967-0645(02)00383-1

have been observed at sea (McDonagh et al., 1999; De Ruijter et al., 1999). The Agulhus rings move partly due to β-induced motion and partly due to advection by the background currents. The speed and tracks of the rings are influenced by bottom topography and interaction with other rings (Byrne et al., 1995; Schouten et al., 2000). Ring translation speeds have been reported to vary between 3 and 16 km/day (Schouten et al., 2000; McDonagh et al., 1999; Goni et al., 1997). Within 10 months after their formation most rings have reached the Walvis Ridge (Schouten et al., 2000).

The Agulhas rings transport warm and saline water from the southern Indian Ocean into the South Atlantic. There, the rings decay and exchange their properties with the surrounding water. Part of this exchanged water crosses the South Atlantic as part of the Benguela Current and feeds into the North Brazil Current. In this way the Agulhas leakage may be a critical link in the global thermohaline circulation (THC) (Gordon, 1986; Weijer et al., 1999). Model studies indicate that Agulhas leakage stimulates and stabilizes the northern meridional overturning circulation (MOC) of the Atlantic Ocean (Weijer et al., 1999, 2001). Estimates for the total heat fluxes involved in this inter-ocean exchange range between 0.1 and 0.8 PW (Gordon, 2001). Salt fluxes range between 0.9×10^5 and 38×10^5 kg/s, assuming a yearly total of six rings (De Ruijter et al., 1999; Gordon, 2001). The large range in heat fluxes results from different assumptions on the temperature of the water that leaves the Atlantic, balancing the warm Agulhus leakage (Gordon, 1985, 2001). Part of this leakage will be balanced on the horizontal plane, as part of the Indian-Atlantic sub-tropical supergyre (De Ruijter, 1982; Gordon et al., 1992), with water from the South Atlantic Current penetrating the Indian Ocean south of the Agulhas Return Current. The other part is balanced by the much colder North Atlantic Deep Water (NADW) and takes part in the MOC (Gordon, 1985).

The main aim of the MARE programme, the Mixing of Agulhas Rings Experiment, is to determine the contribution of the Agulhas rings to the MOC. Satellite altimetry observations have shown that the rings decay to less than half their initial amplitude within 5 months after their shedding (Schouten et al., 2000), while still in the Cape Basin. This part of the rings likely feeds into the MOC. Their remainder drifts westwards and is largely embedded in the supergyre. The observational part of MARE therefore focusses on the decay processes in the Agulhas Basin and Cape Basin (Fig. 1). This was established by three intensive measurement campaigns in which the same Agulhas ring, named Astrid, was visited at different stages of its decay. In this way, a description is obtained of its time-evolution and the dominant decay processes. In this paper we present the observations of the first MARE cruise, by R.V. *Pelagia* in March 2000 (Fig. 1), together with an analysis of several dynamical fields derived from them. During this cruise, we performed for the first time direct observations of the three-dimensional current structure of an Agulhas ring all the way to the bottom, using a lowered acoustic Doppler current profiler (LADCP). Earlier hydrographic observations of Agulhas rings had shown a deep signature of the rings in the density field, not only in Agulhas rings (Olson and Evans, 1986), but also in e.g., Gulf Stream rings (Joyce, 1984). Our observations reveal that the slopes of the isopycnals are connected with a surprisingly strong barotropic component in the velocity field of the ring.

During the MARE-1 cruise, we also carried out two high-resolution hydrographic sections of the upper 200 m of the ring by means of a CTD mounted in an undulating 'Scanfish' platform. At mid-depth the horizontal resolution reached was 1.8 km. This provides a detailed picture of the fine-structure of the ring, particularly across its boundaries where the lateral exchange with the surrounding water takes place. These new types of observations have been combined with 'classic' hydrographic measurements, including nutrients and oxygen, and with satellite altimetry data and surface drifter observations. These data provide an integrated view of the detailed structure of Agulhas ring Astrid in its initial stage of existence.

In order to give a complete description of ring Astrid, we first determine the position of the ring using satellite altimetry. Secondly we show the results of the in situ CTD and LADCP

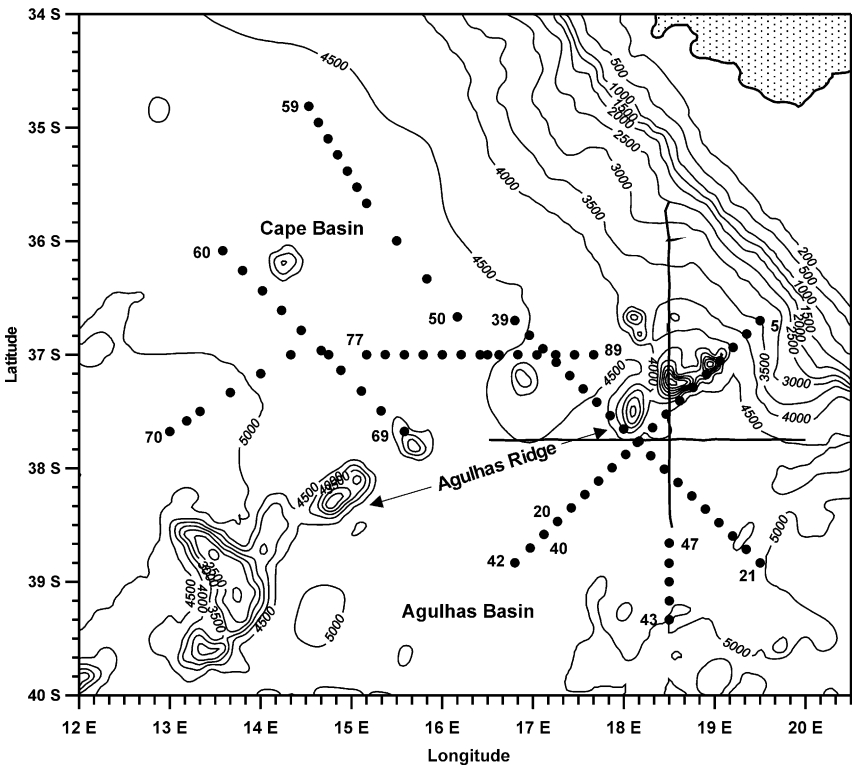

Fig. 1. Bathymetry of the research area of the MARE-1 cruise of R.V. *Pelagia*. The depth is given in m. The positions of CTD stations are indicated with black dots. The sections along which high-resolution surveys of the upper 200 m have been carried out with a CTD mounted in the undulating Scanfish wing are indicated with thick black lines.

measurements and give a water mass analysis. Next the air–sea interaction is discussed, a comparison is given with other observed rings and other aspects are discussed.

2. The data

2.1. Hydrographic data

The MARE-1 cruise of R.V. *Pelagia* ran from Cape Town to Cape Town between 27 February and 19 March 2000, between 34–40°S and 12–20°E, directly south to southwest of Cape of Good Hope, South Africa (Fig. 1). The location of Agulhas rings was determined using satellite altimetry. Based on the altimetry information, the collection of data during the MARE-1 cruise took place in three phases: (1) the search phase for our main MARE ring: Astrid, (2) the intensive CTD survey in and around this ring, and (3) additional CTD observations in the surroundings of Astrid and through a neighbouring MARE ring, Laura.

Just prior to the MARE-1 cruise it was not clear whether the newly formed ring Astrid would continue as a single ring or whether it would be reabsorbed by the retroflection (Byrne et al., 1995) or split up in several smaller rings. For this reason we tried to survey the slightly older and weaker ring Laura as well.

In order to establish the position and extension of ring Astrid in the first phase, a search was performed with a CTD mounted in an undulating Scanfish wing. Towed with a speed of 5–6 knots, the Scanfish wing undulated in a depth range between 15 and 190 m. The horizontal resolution at mid-depth was about 1.8 km. From the two

Scanfish sections (Fig. 1) the centre of the ring was determined and the diameter of the ring was estimated. The accuracy of the temperature and salinity determination of the Scanfish CTD, based on laboratory calibrations, is estimated to amount to 0.003°C and 0.003, respectively. The precision of these parameters, however, is assumed to be about 0.001°C and 0.001.

After establishing the location and extension of ring Astrid in the second phase, a series of CTD casts was carried out at regular intervals of 10 nautical miles in two perpendicular sections running northeast–southwest (stations 5–20, 40–42) and southeast–northwest (stations 21–39) (Fig. 1). Most CTD casts went down to 1000 m, while every fourth cast went to the bottom. The CTD/Rosette system was supplemented with a LADCP, which was operational on most, but not all, CTD stations. Water samples were taken at standard depths for the determination of nutrient and oxygen concentrations and salinity calibrations.

In the third phase of the data collection the region outside of ring Astrid was investigated with the CTD/Rosette system in a number of sections including stations 50–59, 60–69 and 70–89 (see Fig. 1). Satellite altimetry (Fig. 2c) indicated that section 50–59 passed through a region with weak ring activity, that section 60–69 crossed the neighbouring Agulhas ring Laura, and section 70–89 covered the area between the two Agulhas rings Astrid and Laura, including their ring edges. The standard depth of the CTD/Rosette system on stations 70–89 was 1500 m and occasionally bottom casts were performed.

The CTD was a pumped Seabird SBE9/11+ system. The CTD data were recorded on board with 24 Hz. After data processing and calibration the data were reduced to 1 dbar averages. The resulting accuracy of these calibrated and processed CTD data (standard deviation) is estimated to be 1.2 dbar for pressure, 0.001°C for temperature, and 0.001 for (practical) salinity.

From the CTD data additional physical parameters were derived. The density was expressed as density excess γ, calculated according to the International Equation of State for Sea Water 1980: UNESCO (1981, 1985). The potential density excess relative to 0 dbar is indicated as γ_Θ, while γ_n is the potential density excess relative to a pressure of $n \times 1000$ dbar.

Water samples were taken with 5- and 10-dm^3 samplers, mounted in the CTD rack. The water samples were analysed for dissolved phosphate, nitrate, silica, and oxygen. The resulting precision (root mean square of the difference between duplicates) of the chemical analyses is estimated to be 0.4, 0.02, 0.2, and 0.6 μmol/kg for, respectively, oxygen, phosphate, nitrate, and silica.

Since the oxygen saturation concentration depends strongly on temperature, the sub-surface oxygen concentrations not only show the effects of ageing, but also of temperature. In order to separate the temperature effects from the ageing effects on the oxygen concentration, the parameter apparent oxygen utilization (AOU) is often used. AOU is defined as

$$\mathrm{AOU} = [\mathrm{O_{2sat}}] - [\mathrm{O_2}], \quad (1)$$

with $[\mathrm{O_{2sat}}]$ the saturation value of the oxygen concentration $[\mathrm{O_2}]$ in balance with the atmosphere.

The LADCP system consisted of two synchronized self-contained 300 kHz RDI Workhorse broadband ADCPs, one upward looking and one downward. A vertical bin size of 8 m was applied. The accuracy of velocities measured with an LADCP is still difficult to determine, but, referring to (Visbeck (2002), the accuracy of bottom tracked profiles is estimated to be of the order of 1–2 cm/s and the other casts of 5 cm/s.

2.2. Satellite altimetry and drifter tracks

Before the MARE-1 cruise started, the spawning region of Agulhas rings was studied using satellite imagery. Byrne et al. (1995) showed that Agulhas rings can be traced effectively using satellite altimetry. However, they used the altimetry in a less varying region farther west. The TOPEX/Poseidon and ERS-2 satellites sample sea-surface height (SSH). TOPEX/Poseidon has a repeat period of approximately 10 days and ERS-2 of 35 days. These satellite data are used by Colorado Center for Astrodynamics Research (CCAR), http://www-ccar.colorado.edu to generate SSH anomaly maps (Fig. 2), based on 10 days

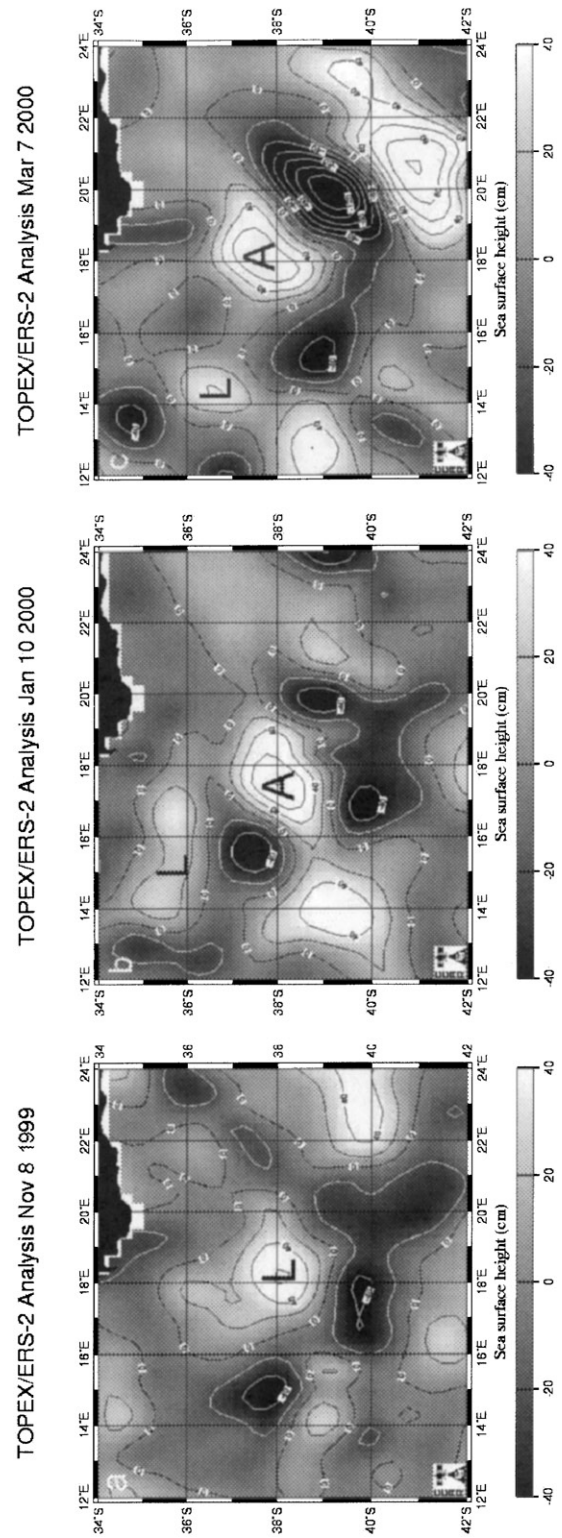

Fig. 2. Sea-surface height anomaly (cm) based on 10 days of TOPEX/Poseidon and 17 days of ERS-2 sampling for the months November 1999 (a), January 2000 (b) and March 2000 (c). It shows the pinching off of ring Laura, indicated with an 'L' (a), ring Astrid, indicated with an 'A' (b), and their positions in March 2000 during the MARE-1 cruise (c).

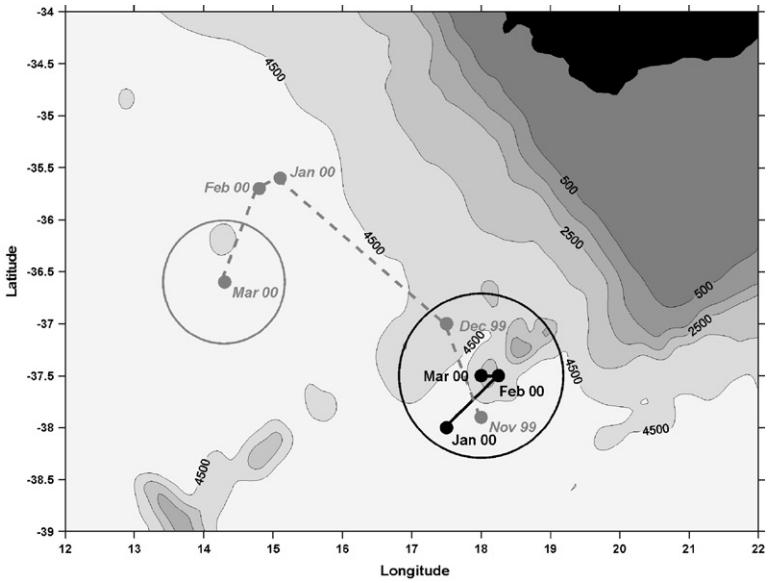

Fig. 3. Track of ring Astrid, from January 2000 until March 2000 (solid line), and of ring Laura, from November 1999 until March 2000 (dashed line). The marks indicate positions 1 month apart, and the circles indicate the extension of the rings Astrid and Laura.

of TOPEX/Poseidon and 17 days of ERS-2 sampling. Anti-cyclonic Agulhas rings are characterized by a positive elevation of the sea surface. Fig. 2 shows the region of the Agulhas Retroflection loop and its western extension before and during the MARE-1 cruise. The grids of the two satellite tracks are relatively coarse and the repeat cycles are relatively long. Therefore, it is not possible to make a very detailed or synoptic SSH anomaly map, especially not in this highly varying region.

2.2.1. *Ring shedding and propagation*

In early November 1999 ring Laura was shed at 38°S, 18°E (Fig. 2a). Laura moved in a northwestward direction to a position of 35°30′S, 15°E in January 2000. Around that time our main MARE ring, Astrid, was pinched off at 38°S, 17°30′E (Fig. 2b). During this cruise, in March 2000, the retroflection loop was situated further south near 41°30′S, 19°E (Fig. 2c). The position of the centre of ring Astrid during MARE-1 was 37°30′S, 18°E. The position of ring Laura during MARE-1 was 37°S, 14°15′E according to the SSH anomaly. Clearly, the interpretation of SSH anomaly data, given above, is somewhat subjective. Sea-surface temperature (SST) images (not shown), however, support our interpretation.

In the first month after its formation, ring Astrid moved northeastwards to the position where it stayed until March (Fig. 3). The scalar drift velocity during this movement was 3 km/day (~3 cm/s). Ring Laura moved initially northwestwards with a maximum drift velocity of 8.6 km/day (10.0 cm/s). After an almost stationary period of a month, ring Laura moved south–southwestwards to its position during the MARE-1 cruise.

Ring Astrid had a maximum SSH anomaly of over +70 cm (Fig. 2c) and can be classified as a 'strong' ring (Schouten et al., 2000). Laura had a maximum SSH anomaly of about +40 cm at the time of the MARE-1 cruise (Fig. 2c). However, the centre of ring Laura, derived from hydrographic observations, appeared not to be located at the position derived from the SSH anomaly. Most probably, ring Laura had moved northwestwards in a relatively short period just prior to the cruise, which was not observable yet in the SSH anomaly interpolation.

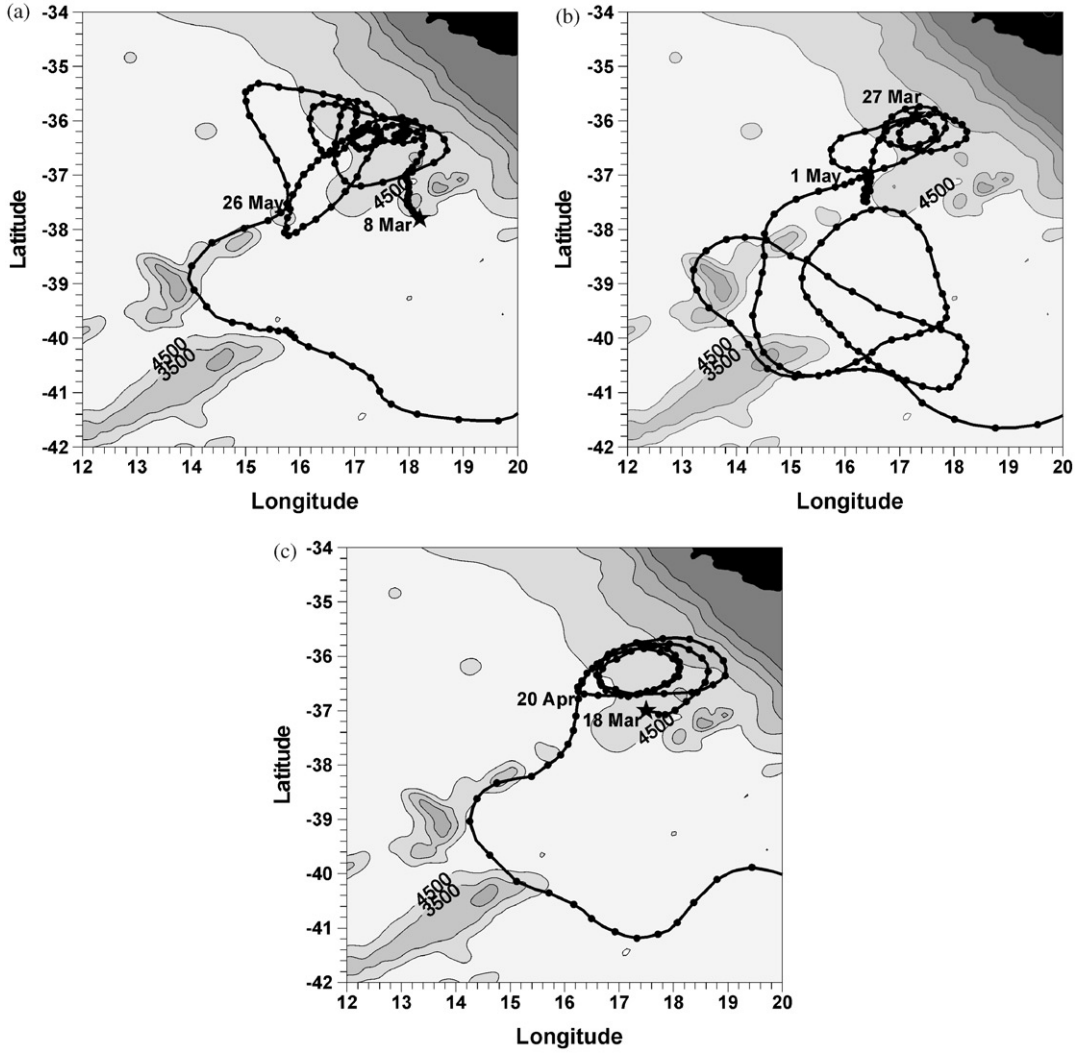

Fig. 4. Tracks of three ARGOS drifters deployed in ring Astrid during the MARE-1 cruise. Dots indicate positions 12 h apart, stars indicate the first recorded positions.

2.2.2. *Drifter tracks*

The position of ring Astrid was followed using drifter tracks. During the MARE-1 cruise, three ARGOS surface drifters were deployed in ring Astrid, in order to follow the ring after this cruise. The drifters were standard spherical WOCE/TOGA drifters, fitted with an 8-m-long holey sock drogue at 15 m. Their positions were followed using the ARGOS system on board the polar orbiting NOAA satellites. In Fig. 4 the drifter tracks are shown. The drifters in Figs. 4a and b were deployed at successive CTD stations near the centre of ring Astrid. Fig. 4a shows that the drifter, and therefore the ring, moved slowly northwards, which is confirmed by the SSH anomalies (not shown). The drifter appeared to be deployed near the centre of the ring because it was not circulating for the first 12 days. Then, the drifter started to gyrate around the centre in an anti-cyclonic sense, until after 11 weeks the drifter left the ring. The drifter in Fig. 4b released its first signal only 19 days after deployment and probably

had followed approximately the same path as the drifter in Fig. 4a. Eight weeks after deployment this drifter left the ring. The third drifter (Fig. 4c) was deployed at the southern edge of the ring at the end of the MARE-1 cruise. This drifter circulated for 5 weeks around the centre before it left the ring. All drifters eventually were found outside the ring where they were absorbed by the Agulhas Retroflection and moved to the east in the Agulhas Return Current. This is an indication of the surface waters detaching from the ring due to a divergent secondary surface circulation (Joyce, 1984) and Ekman drift. However, the surface drifters stayed much longer in the Agulhas ring than for example the RAFOS floats of Schmid et al. (2003) at the Antarctic Intermediate Water (AAIW) level. This can be expected from the much larger tangential velocity of the rings at the surface than at the AAIW level (Flierl, 1981).

3. Hydrographic observations

The horizontal distribution of salinity at a pressure level of 150 dbar (Fig. 5) reveals the position of the saline (and warm) Agulhas ring Astrid, centred near approximately 37°45′S, 18°10′E. Its position closely matches the position of the anti-cyclonic structure derived from the satellite altimetry (see Fig. 2c). The saline core of the ring ($S > 35.55$) is surrounded by less saline water ($S < 35.15$). At the sea surface the ring Astrid is characterized by salinities of over 35.60. Near 36°S, 13°30′E there is evidence of another saline ring, probably related to the second ring observed in the altimetry data, Laura. The latter ring was not surveyed completely, nor in any detail. The fact that Astrid was not completely circular symmetric is probably real, and not due to aliasing due to temporal variations (advection of the ring

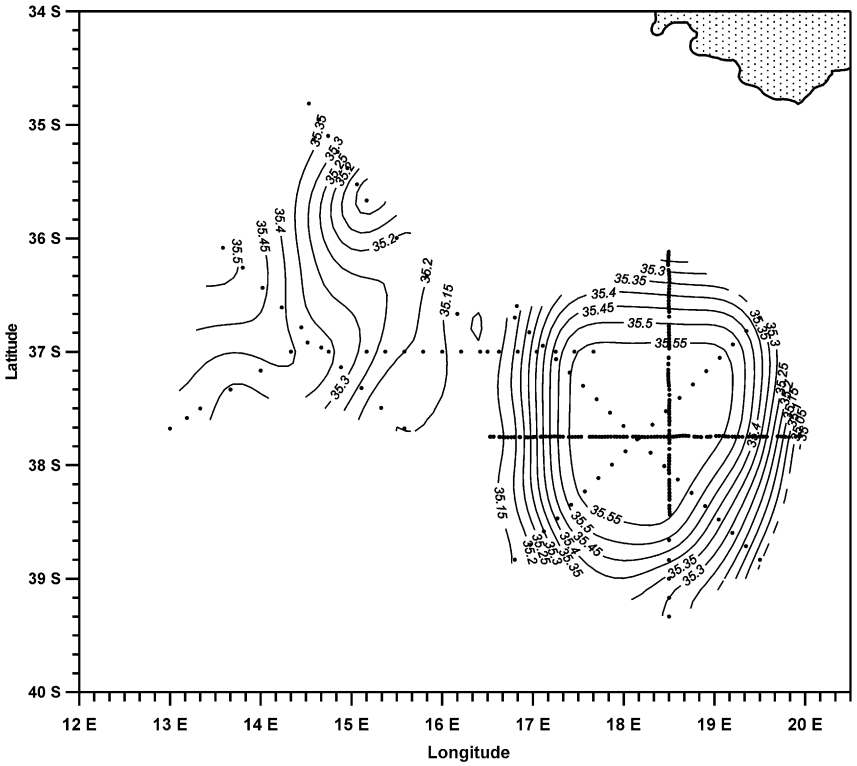

Fig. 5. Horizontal distribution of salinity at a pressure level of 150 dbar. Data from all CTD casts as well as from the Scanfish were used for the construction of this figure. Interpolation on a $0.1 \times 0.1^\circ$ grid was performed by means of a Kriging algorithm. The dots indicate the data points, used for this analysis. After interpolation a two-dimensional Bartlett filter with a width of $0.2 \times 0.2^\circ$ was applied to remove the small-scale structures resulting from the interpolation of the unevenly and anisotropically spaced data points.

during the survey), because it was also observed in observations only one or a few days apart. The salinity minimum near 35°40′S, 15°10′E, was found at the position of a cold and shallow filament which also was observed in SST images (not shown).

The hydrographic structure of the ring, along the CTD section through the centre of ring Astrid from southeast (station 21) to northwest (station 39), is shown in Fig. 6. The bowl-shaped form of the iso-lines, characteristic for anti-cyclonic rings, can be discerned from the surface to the bottom at a pressure of over 4500 dbar. This indicates that interaction of Agulhas rings with the topography of the Agulhas Ridge, and the continental slope may influence the behaviour of the rings in this area. The presence of the warm core ring induces a difference in the SSH between the centre of the ring (the coinciding stations 14 and 30) and the outer boundary (stations 22 and 38) of 82 cm, based on the steric height relative to 4000 dbar. This compares reasonably with the sea-surface topography estimated from the sea-level anomaly determined with satellite altimetry (60–100 cm, see Fig. 2c). In the upper 1500 dbar thermohaline fine-structure, characterized by density compensating inversions of salinity and temperature, with vertical scales of a few tens of metres, is abundant. At pressures of about 500 dbar outside of the ring to 1200 dbar in its centre salinity minima characteristic for the AAIW are observed along the whole section, interspersed with local salinity maxima. The latter are probably due the presence of remnants of Red-Sea Intermediate Water (RSW) from the Agulhas Current (Beal et al., 2000). At pressures between 2500 and 3000 dbar a local salinity maximum, connected with the core of NADW, is observed. Here a small but consistent horizontal salinity gradient is encountered, with highest salinities northwest of Astrid, north of the Agulhas Ridge.

Vertical hydrographic sections through Astrid with potential density as a vertical co-ordinate show the difference in hydrographic properties between the ring and its surroundings (Fig. 7). The density interval shown in Fig. 7 represents the layer between the top of the thermocline and the AAIW layer. Salinity at levels above the $\gamma_\Theta = 26.7$ kg/m^3 isopycnal is systematically higher in the core of the ring (stations 24–37) than in its surroundings. The maximum salinity contrast is observed at a potential density of $\gamma_\Theta \approx 26.0$ kg/m^3 ($\Delta S \approx 0.6$). With potential density as vertical co-ordinate this implies that the centre of the ring is also warmer than its surroundings. At stations 21–24, and 37–39 cold low-salinity cores are observed, possibly intruding into the core of the ring by isopycnal advection. Salinity inversions connected with such thermohaline intrusions are also observed everywhere on the other sections near the edge of the ring. Smaller-scale intrusions occasionally also are observed at stations in the ring's centre. Because of the co-occurring temperature structure, with occasional temperature inversions, this thermohaline fine-structure is hardly reflected in the density stratification. Below the $\gamma_\Theta = 26.7$ kg/m^3 isopycnal, systematic salinity differences between the core of the ring and its surroundings disappear, although the non-horizontal, wave-like character of the isohalines in Fig. 7a show that at these deeper levels still some thermohaline structure is present, but apparently not related to the ring ($\Delta S \approx 0.05$).

As a quasi-conservative parameter, indicative of the static stability of the water column, we use the potential vorticity, λ, defined as

$$\lambda = \frac{(f + \zeta)N^2}{g}, \tag{2}$$

where f is the Coriolis parameter, ζ is the relative vorticity, N is the Brunt–Väisälä frequency, and g is the gravitational acceleration. In order to suppress the effects of noise in low-stability areas, the vertical density gradient, used to determine N, is estimated from a finite difference over 50 dbar intervals. For the presentation of the potential vorticity we assume that the value of ζ is negligible compared with f. In that case λ is a large-scale potential vorticity.

As can be expected for an anti-cyclonic ring, the magnitude of the large-scale potential vorticity in the ring is lower than in its surroundings (Fig. 7b). Above the $\gamma_\Theta = 26.7$ kg/m^3 isopycnal the large-scale potential vorticity varies with a factor 3–10 between the centre of the ring and its surroundings. Below that isopycnal no systematic difference

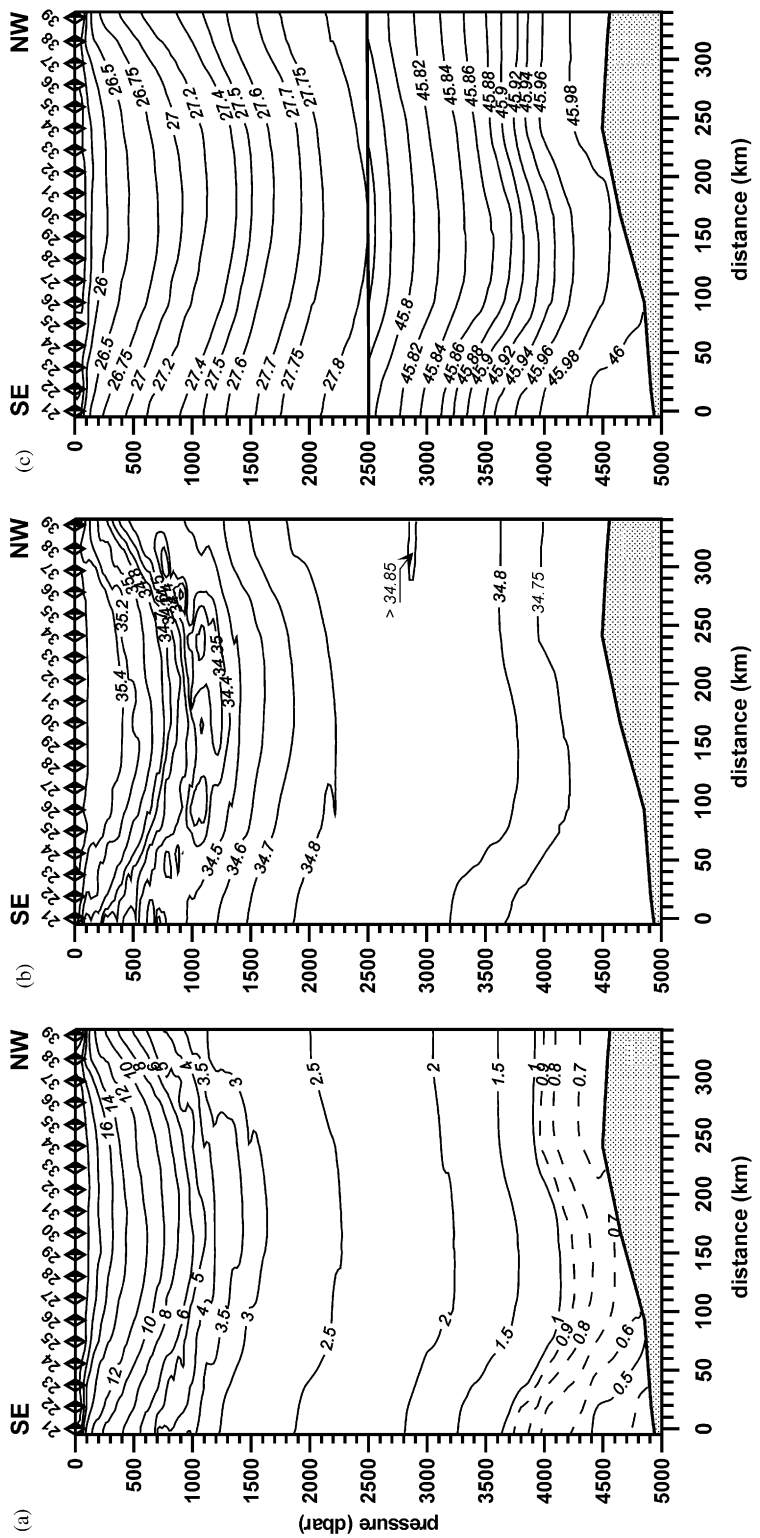

Fig. 6. Vertical sections of potential temperature (a), salinity (b), and potential density excess (c). In (c) the upper 2500 dbar give the excess γ_Θ relative to a reference level of 0 dbar, while in the lowest 2500 dbar the excess γ_4 relative to a reference pressure of 4000 dbar is depicted. The horizontal resolution of the observations is about 18 km in the upper 1000 dbar and 55 km below that pressure. The station numbers are indicated on top.

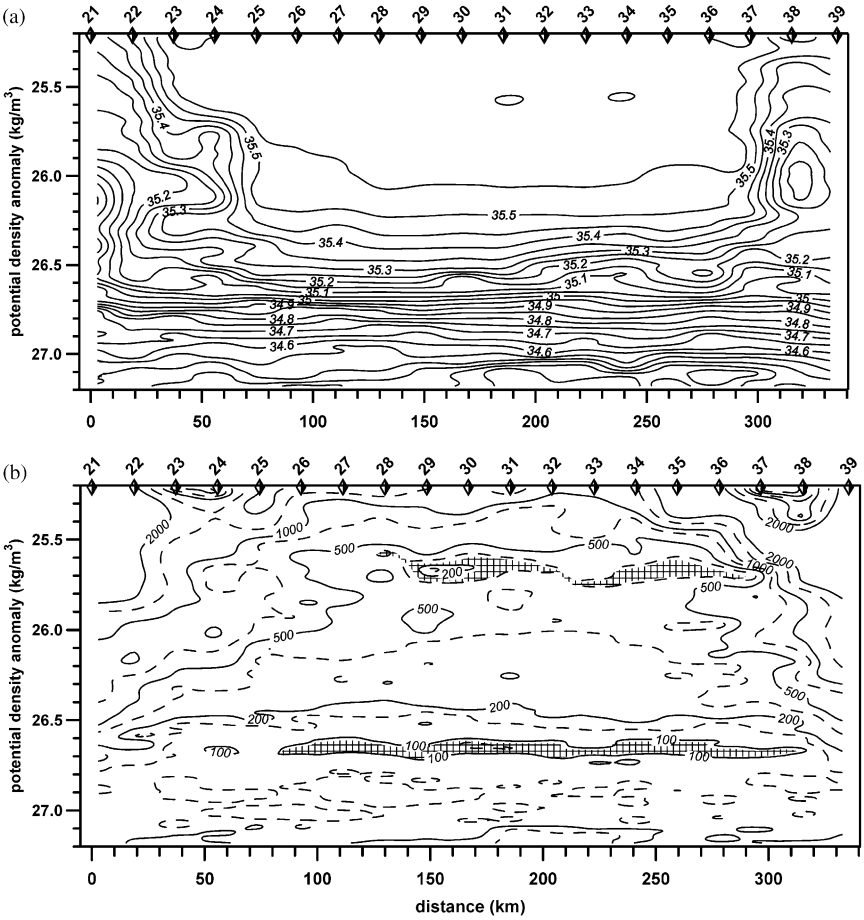

Fig. 7. Vertical sections through the ring Astrid with the potential density excess γ_Θ as vertical co-ordinate: (a) salinity, (b) the magnitude of the (negative) large-scale potential vorticity. The dashed areas in (b) show the local minima in potential vorticity. The density interval in this figure is representative for the 100–1100 dbar layer in the centre of the ring, and for the 50–500 dbar layer at the edges of the ring (stations 21 and 39). The section runs from southeast to northwest. The horizontal resolution of the observations is about 18 km. The large-scale potential vorticity λ is defined as $\lambda = (fN^2/g)$ where f is the Coriolis parameter, N the Brunt–Väisälä frequency, and g the gravitational acceleration. Units of λ are in 10^{-12} ms^{-1}. The station numbers are indicated at the top of the panels.

between the ring and its surroundings can be discerned, similar to the salinity. The top of the thermocline in the surrounding water is found at higher densities, and is overall more stratified than the thermocline in the ring. Inside the ring two local minima of the magnitude of the large-scale potential vorticity can be discerned, one at $\gamma_\Theta \approx 26.65$ kg/m^3 ($\Theta \approx 12^\circ$C), and a shallower one at $\gamma_\Theta \approx 25.60$ kg/m^3 ($\Theta \approx 18^\circ$C). The 18°C minimum is not found as a coherent layer outside of the ring. Below the lower minimum the vertical distribution of large-scale potential vorticity seems to be similar in the ring and in the surrounding waters.

The vertical section through the upper 200 dbar, derived from the Scanfish survey (Fig. 8), shows a very homogeneous mixed layer in the ring, extending to pressures over ~90 dbar in its centre. Both the temperature and the salinity in the upper 90 dbar in the centre of the ring are vertically very homogeneous, with typical standard deviations of 0.005°C and 0.001, respectively. Outside the

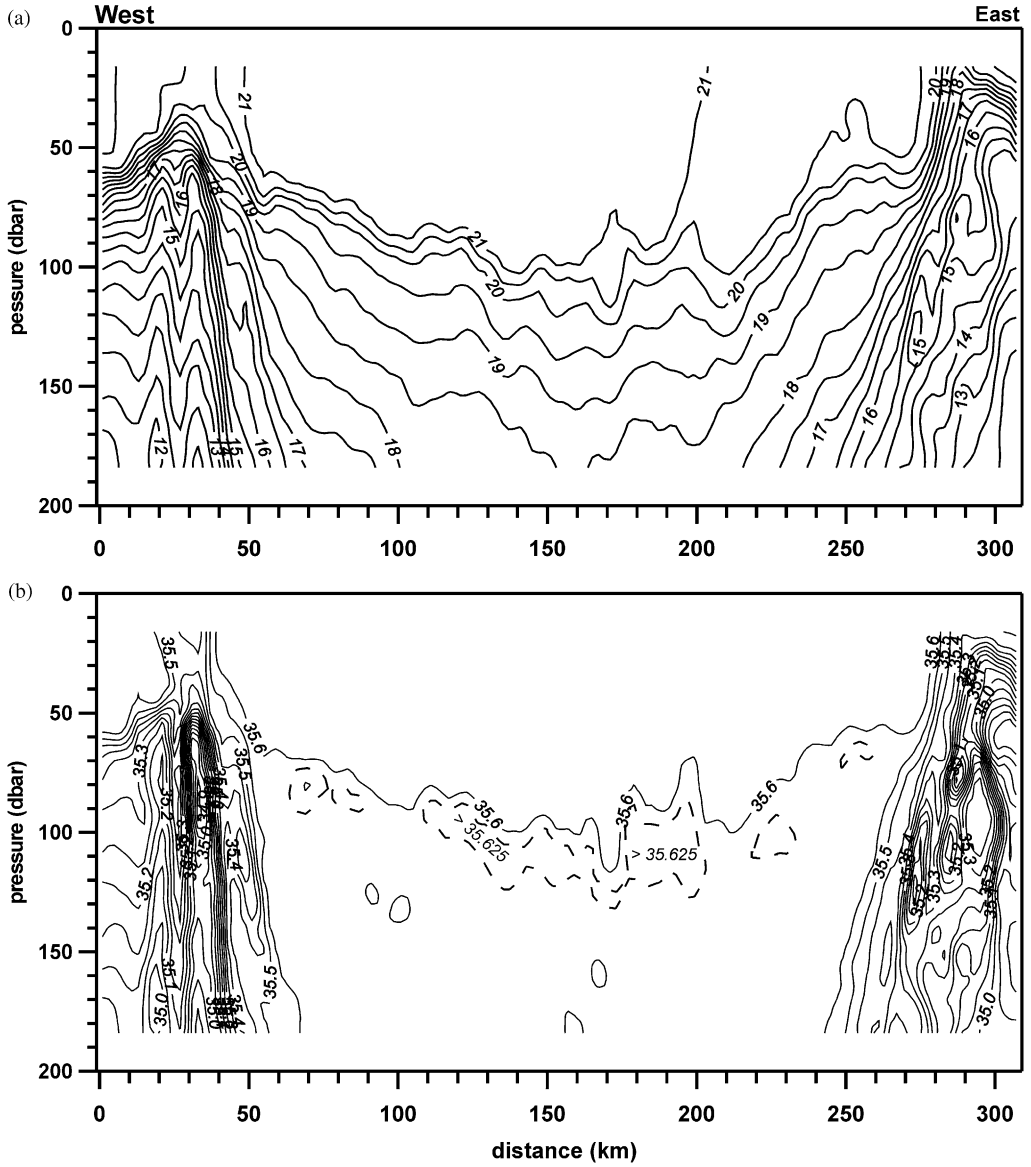

Fig. 8. Vertical distribution of temperature (a) and salinity (b) along the west–east Scanfish section through ring Astrid. The horizontal resolution of the Scanfish survey at mid-depth amounts to 1.8 km. The isotherm distance in (a) is 0.5°C; the isohaline distance in (b) is 0.05. In (b) an additional 35.625 isohaline has been drawn to mark the salinity maximum at the top of the thermocline (dashed line).

anti-cyclonic ring the maximum mixed-layer depth is generally much less than 50 dbar. This indicates that convective mixing, driven by the sea-surface heat loss, is quite active in modifying the warm upper waters in the ring, even in the summer situation presented here. Salinity in the upper 200 dbar of the ring shows little vertical variation, with a slight salinity maximum ($S > 35.625$) just below the top of the thermocline. Temperature in the ring shows a steady decrease from the top of the thermocline downwards.

The Scanfish survey crossed the boundary of the ring with large salinity gradients three times, at the northern, western, and eastern side (Fig. 5).

The salinity distribution across this ring boundary (Fig. 9) clearly shows the fine-structure. Alternating bands of more saline or fresher water are observed to encircle the ring. These bands are more or less aligned along isopycnal surfaces where temperature compensates the effect of salinity on density. The typical horizontal, radial scale of the fine structure is 5–6 km, definitely less than the distance between successive CTD stations. However, along the sloping isopycnals some bands can be followed over longer horizontal distances, up to about 40 km. It cannot be established what the tangential length scale of the fine-structure is, because of the limited resolution in that direction. Due to the presence of the fine-structure bands diapycnal gradients are strongly enhanced. It can be expected that this enhancement of local gradients is the stirring action that leads to increased turbulent mixing, which forms a pathway for exchange of heat and salt between the Agulhas rings and their environment. As shown below, the fine-structure is found in a region with large vertical velocity shear, due to the high horizontal density gradients.

The plots of salinity and large-scale potential vorticity versus potential temperature (Fig. 10) confirm that the systematic water mass differences between the ring Astrid and the surrounding ocean is restricted to the part of the water column with potential temperature above 12°C. In the centre of the ring this isotherm is found at approximately 600 dbar, whereas it is found between 140 and 200 dbar outside the ring. At lower temperatures the Θ–S properties of the ring and its surroundings hardly differ. The minimum of $|\lambda|$ near the 18°C isotherm is characteristic for the pycnostad in the upper parts of the water column within the ring at about 210 dbar. Outside of the ring this isotherm is situated in the seasonal thermocline with considerable stratification. Near the 12°C isotherm the waters surrounding the ring also show a local minimum of $|\lambda|$. These minima in large-scale potential vorticity are characteristic for Mode Waters, which are formed by convective mixing, driven by atmospheric cooling (McCartney, 1982). The local salinity minimum of the intermediate water near $\Theta = 4.1$°C, is connected with a change in the slope of the Θ–λ curve, while the local salinity maximum near $\Theta = 2.1$°C, characteristic for the core of NADW, coincides with a local potential vorticity minimum.

The bio-geochemical data, plotted versus potential temperature (Fig. 11), show that above the 12°C isotherm, at constant temperature levels, the ring contains more nutrients, and less oxygen (higher AOU) than the surrounding water. Apparently the water mass in the ring appears more 'aged' than the water outside the ring. However, because of the negative correlation of potential temperature and nutrient concentrations, the concentrations of nutrients at a fixed depth level are smaller in the warm ring than in its colder surroundings. Near the temperature levels where minima in $|\lambda|$ are found ($\Theta \approx 18$°C and 12°C) the water inside the ring also has local maxima in oxygen (minima in AOU). At the 12°C isotherm the oxygen concentration in the ring is larger than outside of the ring.

4. Water mass analysis

The water mass in the ring consists of warm surface water, a thermocline with low-stability Mode Waters near $\Theta = 18$°C and 12°C, and underlying intermediate water, dominated by AAIW, but with remnants of RSW (Fig. 10). The water in the thermocline is named Southern Indian Ocean Central Water (SICW; Fine et al., 1988; McDonagh and Heywood, 1999). At deeper levels the high-salinity NADW core is observed, overlying the fresher Antarctic Bottom Water with $\Theta < 1$°C.

The surface mixed layer in the ring was very homogeneous, which is attributed to active convective mixing. This mixing was driven by a heat loss of the order of 54 W/m^2 over the ring. So, even in austral summer the water in the young Agulhas ring was modified convectively. The oxygen concentration in the mixed layer is close to saturation (AOU ≈ 3 μmol/kg). The low-stability 18°C Mode Water at ~ 200 m was nowhere connected with the surface mixed layer. Apparently it got its properties during convective mixing before it left the Retroflection region. Such Subtropical Mode Water (STMW) with a potential

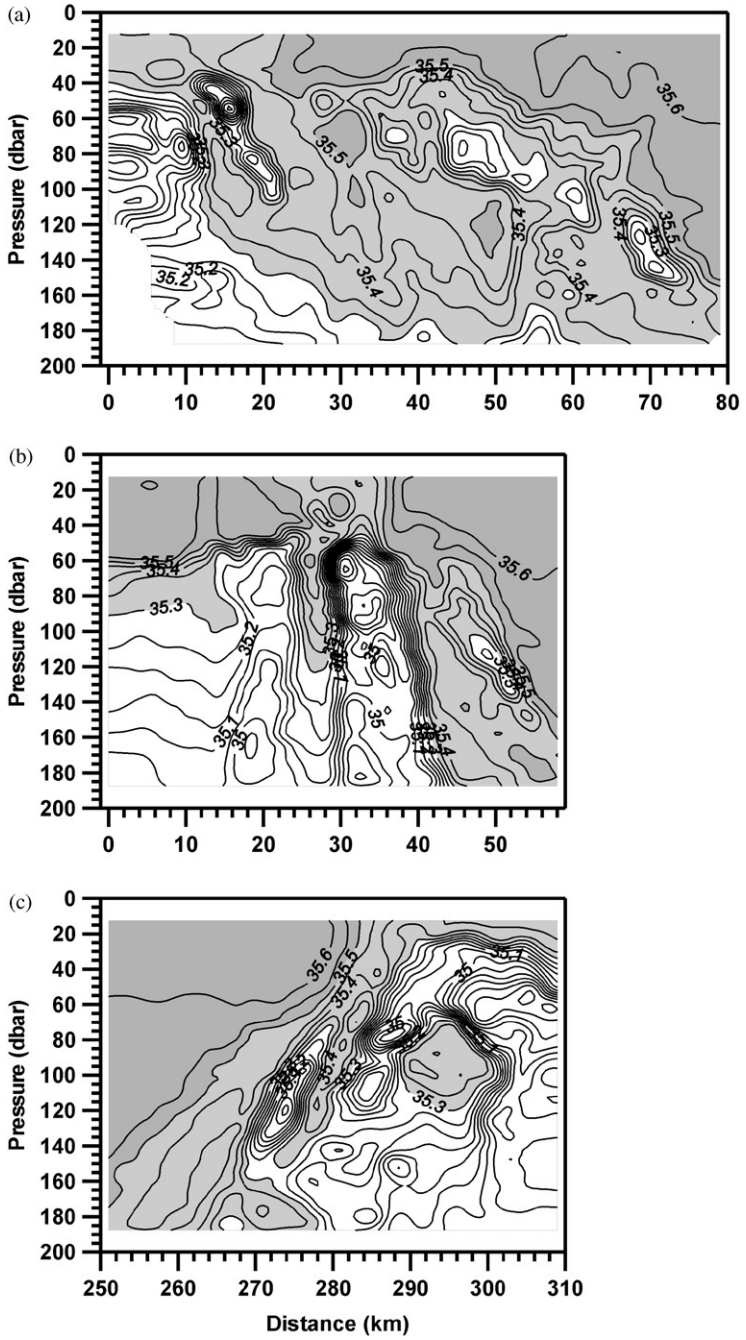

Fig. 9. Vertical sections of the salinity across the boundary of the ring Astrid, based on the Scanfish survey: (a) the northern boundary, (b) the western boundary, and (c) the eastern boundary. Dark shading is indicative for the water in the centre of the ring, no shading for the surroundings of the ring. These boundaries coincide with the areas where the Scanfish lines cross the large salinity gradient in Fig. 5.

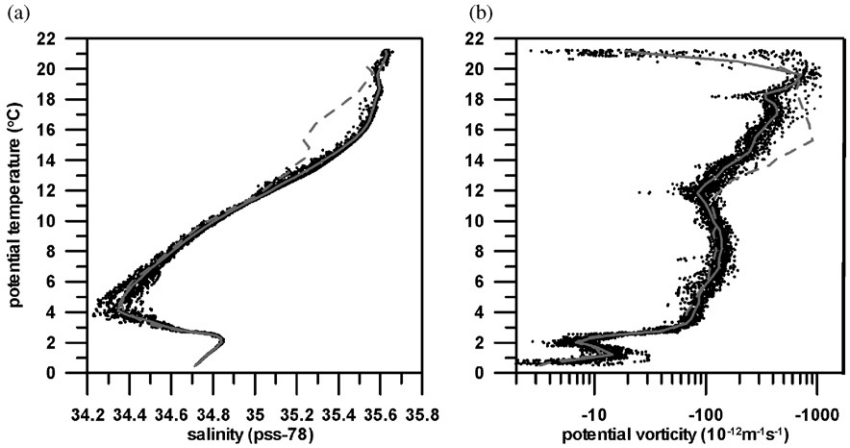

Fig. 10. Plots of salinity (a) and large-scale potential vorticity (b) versus potential temperature. The dots show the data points from the ring Astrid, sub-sampled every 10 dbar. The full line indicates the mean curve in the ring, and the dashed line the mean curve in the direct surroundings of the ring.

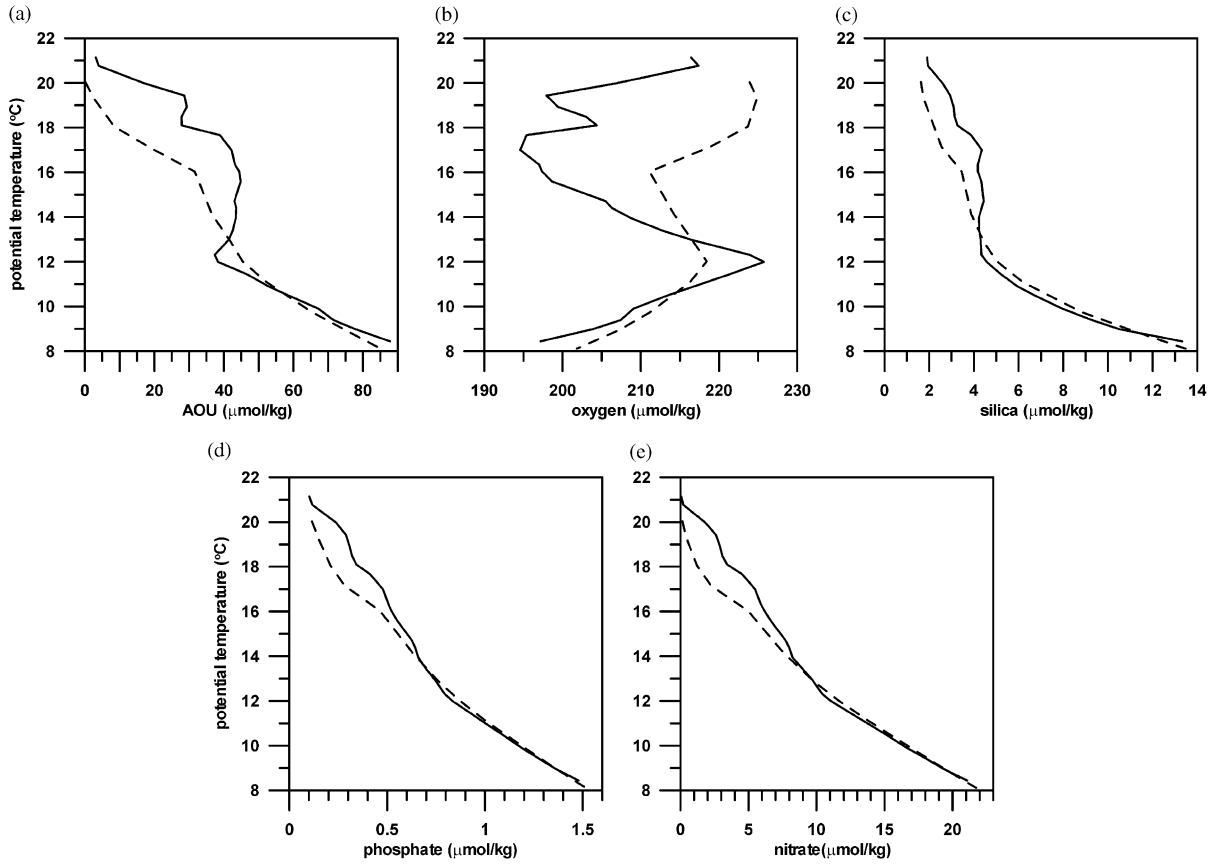

Fig. 11. Plots of apparent oxygen utilization (a), dissolved oxygen (b), dissolved silica (c), phosphate (d), and nitrate (e) versus potential temperature. The full line depicts the mean water mass properties inside ring Astrid, the dashed line represents the mean properties in the waters directly surrounding the ring.

temperature of 17–18°C is known to be formed in the sub-tropical sub-gyre in the southwestern Indian Ocean, preferentially over the Crozet Basin and the Mozambique Basin (McCartney, 1982; Gordon et al., 1987; Fine, 1993). After formation in winter the STMW subducts into the seasonal thermocline below the sub-tropical surface water further north, before it is brought to the retroflection by the anti-cyclonic circulation in the southwestern sub-gyre. Its small but characteristic local oxygen maximum (Fig. 11) is indicative for recent interaction with the atmosphere. Outside of the ring, this STMW is not found. It is known that in winter the near surface waters in Agulhas rings can be modified by convective cooling in the South Atlantic, including the STMW from the southwestern Indian Ocean, to a temperature below 17°C at a depth of over 200 m (Gordon et al. 1987; Garzoli et al., 1999).

The 12°C Mode Water is identified as Sub-Antarctic Mode Water (SAMW). This water type is formed near the Sub-Antarctic Front in the anticyclonic gyre of the South Indian Ocean. Near Australia a dense variety of SAMW is formed, with a density excess of approximately $\gamma_\Theta = 26.75$–$26.85\ \mathrm{kg/m^3}$ (Fine, 1993; Stramma and Lutjeharms, 1997). A lighter variety of SAMW is formed further west over the Crozet Basin, under the influence of the southwestern sub-gyre (Fine et al., 1988; Fine, 1993; Stramma and Lutjeharms, 1997), with a density excess $\gamma_\Theta = 26.6$–$26.7\ \mathrm{kg/m^3}$. This Mode Water also is characterized by a local oxygen maximum, as observed during the MARE-1 survey (Fig. 11). The water in the thermocline of the ring above the AAIW salinity minimum is assumed to be Southern Indian Central Water, in which STMW and SAMW are found as pycnostads. However, the SAMW and AAIW from the Indian Ocean and from the Southern Atlantic hardly differ in their hydrographic properties because of considerable exchange between these oceans via the Agulhas Return Current (Fine et al., 1988). This is probably a reason why below the SAMW level no systematic differences of water mass properties between the ring and its surroundings can be observed.

The water outside the ring with temperatures above 12°C is found in the upper 175 m. That is in or close to the photic zone where primary production takes place, inducing a rise on the oxygen concentration and a reduction in the nutrient concentrations. Fluorescence measurements confirm a resulting high chlorophyll concentration outside the ring. That is probably the reason why the water outside the ring is apparently less 'aged' than the water at similar temperatures in the ring (Fig. 11) since primary production will reduce nutrient concentrations and enhance the oxygen concentration.

The difference between the water mass properties in an Agulhas ring and its Atlantic surroundings can only be maintained if the water mass in the ring is trapped for a considerable part, preventing surrounding water to enter the ring when the ring is translated (Flierl, 1981). Apparently this has happened with the water above the SAMW at 12°C, located at a depth of about 650 m in the centre of the gyre (Fig. 6a).

5. LADCP measurements

The northeastward velocity component perpendicular to the section from southeast to northwest, measured with the LADCP (Fig. 12a), shows that along this section the velocity around the ring is anti-cyclonic from top to bottom. At station 22, positioned at the outer edge of the ring, the velocity decreases from 0.4 m/s at the surface towards zero at about 1500 m. At the other three stations, positioned within the ring (26 and 34) and at the opposite edge (38), three depth intervals with different shear characteristics can be discriminated. In the upper 1000 m the vertical shear is relatively large and the velocity decreases from 0.9 m/s to values of the order of 0.2 m/s. Between $\sim$1000 and $\sim$3500 m the velocity is approximately constant, while below 3500 m the velocity decreases towards the bottom. At some stations near the centre of the ring LADCP observations were lacking (28 and 31–34, for station 30 the observations from station 14 at the same position have been used). There the velocity has been approximated by the geostrophic velocity with a reference velocity at 1000 dbar, estimated by means of horizontal linear interpolation of the

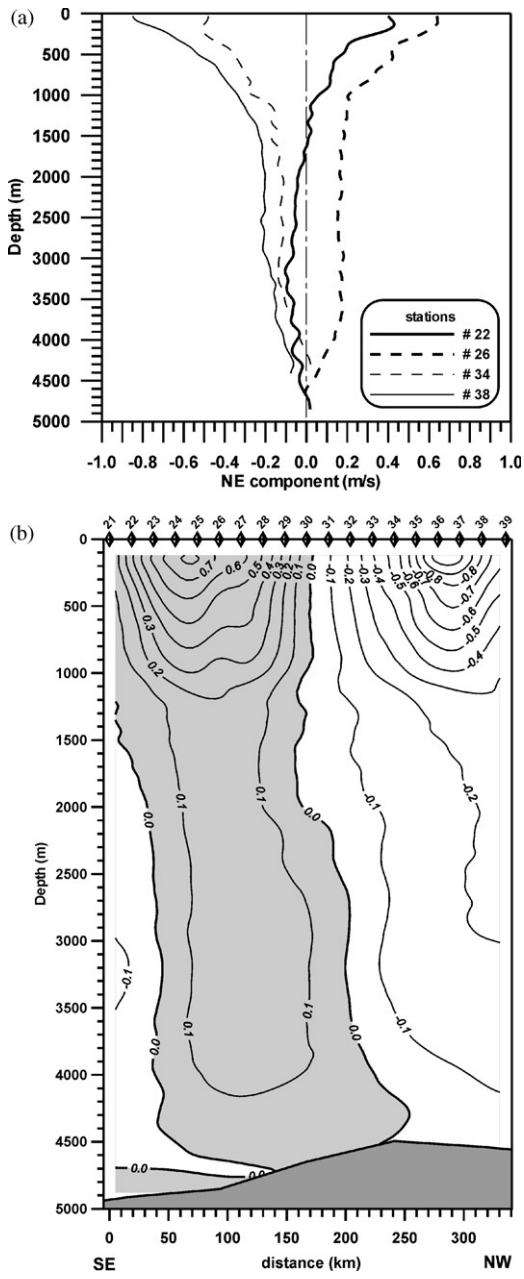

Fig. 12. Northeastward velocity component, perpendicular to the southeast towards northwest hydrographic section through the ring: (a) velocity measured with the LADCP at four stations as a function of depth, (b) section of the NE velocity component (m/s) through the ring Astrid from station 21 to station 39. The shaded area shows the positive velocities (towards northeast). Station numbers are shown at the top.

LADCP velocities. This has allowed us to draw a velocity section across the ring Astrid (Fig. 12b). The maximum surface velocities are found near stations 25 and 37 separated by a distance of 220 km. Halfway between these stations, at station 30, the northeastward velocity is approximately zero from top to bottom. The relatively large vertical shear in the deepest kilometre cannot be ascribed to bottom friction; this layer is too thick. Possibly the near-bottom shear is due to downward Ekman pumping above the bottom. With the existing stratification that will lead to vortex stretching in the lowest layer of the water column. With a negative value of f and a positive value of ζ conservation of potential vorticity then will lead to a decrease of the relative vorticity and therefore of the tangential velocity in the lowest parts of the ring.

The LADCP observations at different depth levels (Fig. 13) show maximum anti-cylonic velocities of over 1.0 m/s in the top of the thermocline at 150 m, and over 0.5 m/s at a depth of 900 m. At a depth of 2500 m, near the levels of the NADW core, as well as in the near-bottom layers at 4000 m the rotation is still anti-cyclonic although deformed, with maximum velocities of 0.2 and 0.17 m/s, respectively. Especially in the northeastern part of the ring the deep velocity is oriented more or less parallel to the topography. This causes the centre of the rotating flow to shift in a west to northwestward direction, relative to the centre of the ring in the upper 1000 m. The lower part of the continental slope is found near the northeastern station with a water depth of approximately 4000 m. There the observed velocity ($|\vec{v}| \approx 0.1$ m/s), located within 100 m from the bottom, is directed parallel to the continental slope. The northern half of ring Astrid overlies several seamounts, extending well above the 2000 m depth level. The velocity vector near 37°15′S, 18°40′E is directed in the northeastward direction, parallel to the slope of the ridge of seamounts just north of that position. This indicates that the deep, relatively strong currents (0.1–0.17 m/s) probably interact with the topography. Numerical experiments indicate that the type of interaction with the bottom varies with the vertical shear in the ring, inhibiting

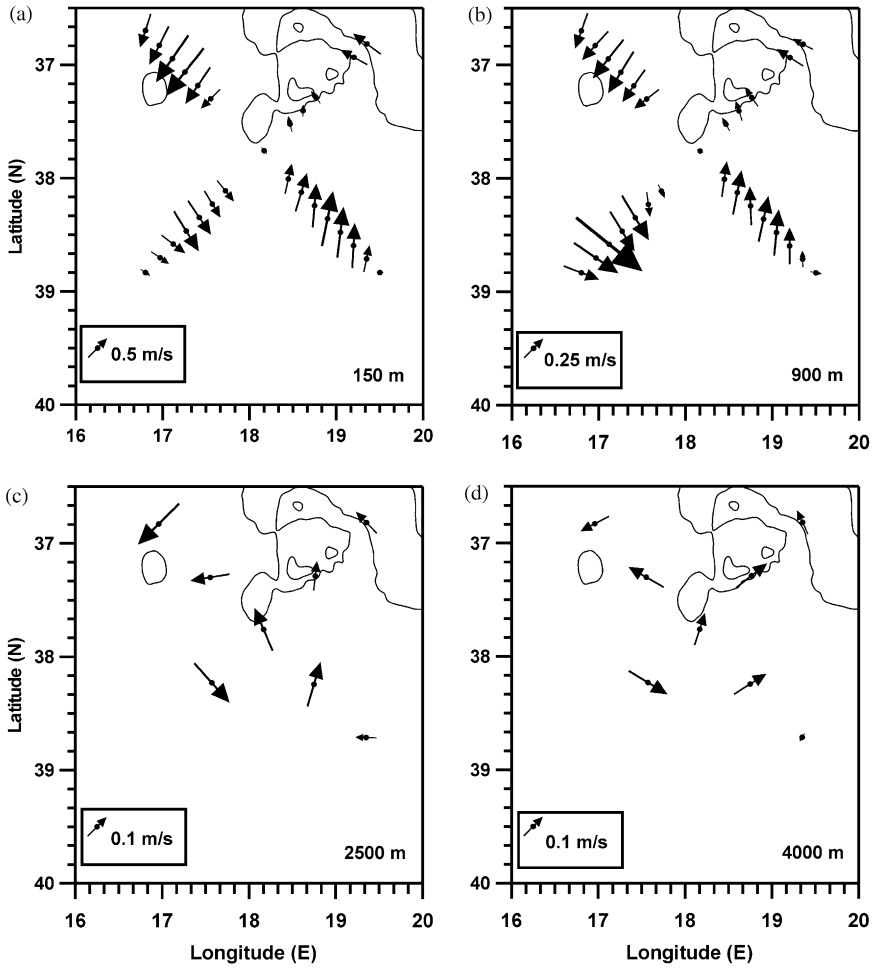

Fig. 13. Velocity vectors from the LADCP, at depths of 150 m (a), 900 m (b), 2500 m (c), and 4000 m (d). Before sub-sampling at the depth levels, the profiles of the velocity components have been smoothed by means of a Bartlett filter with a width of 200 m. Note that the vector scale at the successive depth levels changes. For reference the 4000 and 2000 depth contours have been added.

near-barotropic rings to cross ridges (Kamenkovich et al., 1996). Possibly the observed stalling of the ring Astrid near the Agulhas Ridge, for at least 6 months after the survey described here, is due to the considerable barotropic component in the ring.

Fig. 14a shows that solid body rotation is a reasonable approximation for the motion in the centre of the gyre (between 50 and 220 km), which allows us to use a linear regression of the tangential velocity perpendicular to the hydrographic sections (thick straight lines in Fig. 14a) to estimate the lateral velocity shear and the relative vorticity. With the approximation that the ring is circularly symmetric, we calculate the relative vorticity ζ from the velocity, as shown in Fig. 14a. In a circularly symmetric system, ζ is defined as

$$\zeta = \frac{1}{r}\frac{\partial rV}{\partial r}, \tag{3}$$

where r is the radius and V is the tangential velocity, defined positive counter-clockwise. This implies that a solid body rotation with angular velocity ω has a relative vorticity $\zeta = 2\omega$. At a pressure of 100 m the mean relative vorticity in the

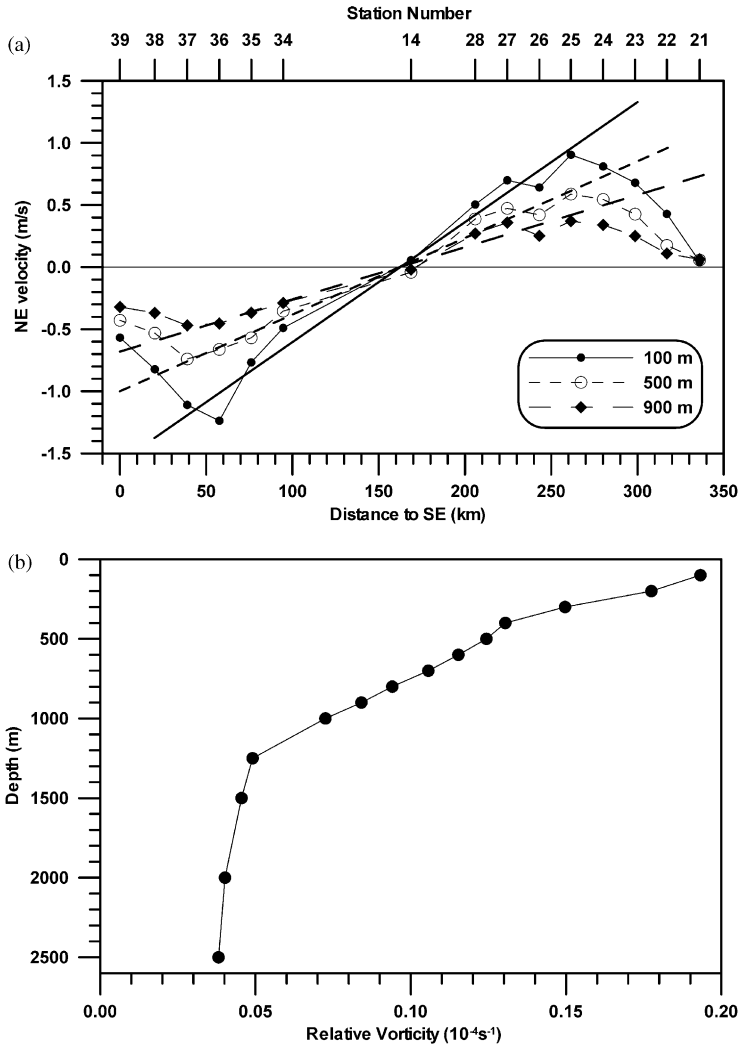

Fig. 14. (a) Northeastward velocity component measured with the LADCP, perpendicular to the hydrographic section from station 21 to station 39 at 100, 500 and 900 m depth (see legend). The thick lines show the linear regression which approximates a solid body rotation in the interior of ring Astrid. (b) The relative vorticity of the solid body rotation in the centre of ring Astrid as a function of depth. This parameter has been derived from the linear regression as shown in (a). It clearly reveals the barotropic core of the ring and the baroclinic component above roughly, 1200 m.

centre of the ring (Fig. 14b), between the velocity maxima, amounts to 0.19×10^{-4} s^{-1} ($\pm 0.01 \times 10^{-4}$ s^{-1}). This is 21% of the magnitude of the local Coriolis parameter f which amounts to $f = -0.89 \times 10^{-4}$ s^{-1}. In the southeastern end of the section (stations 21–24), where the section extended well beyond the velocity maximum (Fig. 13b), ζ becomes small, but negative, with a mean value of -0.02×10^{-4} s^{-1} ($\pm 0.01 \times 10^{-4}$ s^{-1}). At pressure levels of 500 and 900 dbar the mean relative vorticity in the centre of the ring amounts to, respectively, 14% and 9% of the Coriolis parameter, while below 1200 m the relative vorticity is nearly constant with a value of about 0.04×10^{-4} s^{-1} ($\pm 0.01 \times 10^{-4}$ s^{-1}). So the absolute vorticity $f + \zeta$ varies within only about

30% between the ring and its surroundings. The large-scale potential vorticity in Fig. 7b shows differences between the centre of the ring and its surroundings of the order of a factor 3–10. This difference is much larger than can be ascribed to the influence of the variation of ζ between the ring and its surroundings. It is due to the large difference in vertical stratification between the ring and the surrounding water. This should be ascribed to differences in the source regions and properties of the respective water masses.

6. Air–sea interaction data and analysis

Agulhas rings like Astrid are modified by lateral interaction with the surrounding water as well as by air–sea interaction. The vertical homogeneity of the surface mixed layer, presented above, is an indication of convective mixing due to a sea-surface heat loss. In order to determine the net sea-surface heat budget of ring Astrid, meteorological and sea-surface parameters have been measured every 10 s. The measured parameters were sea-surface bulk temperature and salinity, air temperature and humidity, wind speed and direction, incoming short-wave (visible) and long-wave (infrared) radiation, and air pressure. These high-frequency observations were condensed to 10 min average values.

Using the bulk method of Fairall et al. (1996), the turbulent fluxes of momentum, sensible and latent heat were calculated in an iterative process, starting with a value of the flux, corresponding to neutral atmospheric stability. With these fluxes a first guess of the Monin–Obukov length and the stability parameter could be obtained. The stability parameter is equivalent with the flux Richardson number and represents the ratio of the work done by the buoyant force and the rate of shear production of turbulent energy. These parameters, which show whether atmospheric conditions at the surface are stable or unstable, were used for a following iteration until the required accuracy was obtained. The algorithm has separate modules to calculate the real (absolute) sea-surface temperature, T_s (skin temperature), from the measured bulk sea-surface temperature measured at approximately 4.5 m below the surface, and to calculate the meteorological parameters at a standard height of 10 m. Outgoing infrared radiation was calculated as a function of T_s ($-5.7 \times 10^{-8}\ T_s^4$). The outgoing or reflected visible radiation was assumed to be a fixed percentage (7%) of the incoming visible radiation.

Most of the hydrographic sampling in ring Astrid and its surrounding water was completed between 29 February and 11 March 2000. For this period the 10-min-averaged meteorological parameters and the derived heat flux components are shown in Figs. 15 and 16. Table 1 gives the mean parameters with standard deviation, minimum and maximum values for the observational period. For the total observational period, the mean net heat budget of the sea surface amounts to $-54\ W/m^2$. This is mainly due to the large mean latent heat flux ($-180\ W/m^2$), which exceeds the mean net radiation flux ($158\ W/m^2$) in magnitude. The net heat loss is 30% lower than the summer climatological mean for the area northwest of the Agulhas Retroflection (Mey et al., 1990). With a net heat loss of the order of $50\ W/m^2$, a mixed layer with a thickness of about 100 m as encountered in Astrid will cool with only about $0.3^\circ C$/month. Outside Astrid, where the mixed-layer depth was less than 50 m, the cooling rate will surpass $0.6^\circ C$/month, maintaining the sea-surface temperature difference between the ring and its surroundings.

The standard deviation around the mean sea-surface temperature of $20.5^\circ C$ amounts to $0.6^\circ C$, about a factor 3 smaller than the standard deviation of the air temperature. The sea-surface temperature shows some sharp drops (Fig. 15, e.g. March 2, March 3, and March 6). An analysis of simultaneous satellite-SST images of the research area (not shown) reveals that these temperature drops are related to a cool filament of Sub-Antarctic Surface Water (SAASW) drawn from the Sub-Antarctic Front. This water is the cool, fresh surface and sub-surface water surrounding Astrid (Fig. 10a). Similar SAASW filaments have been reported to surround other Agulhas rings (van Ballegooyen et al., 1994). No systematical changes of the net heat budget have been observed at the times when the R.V. *Pelagia* crossed the front between the cold filament and the warm surface water in Astrid. However, strong

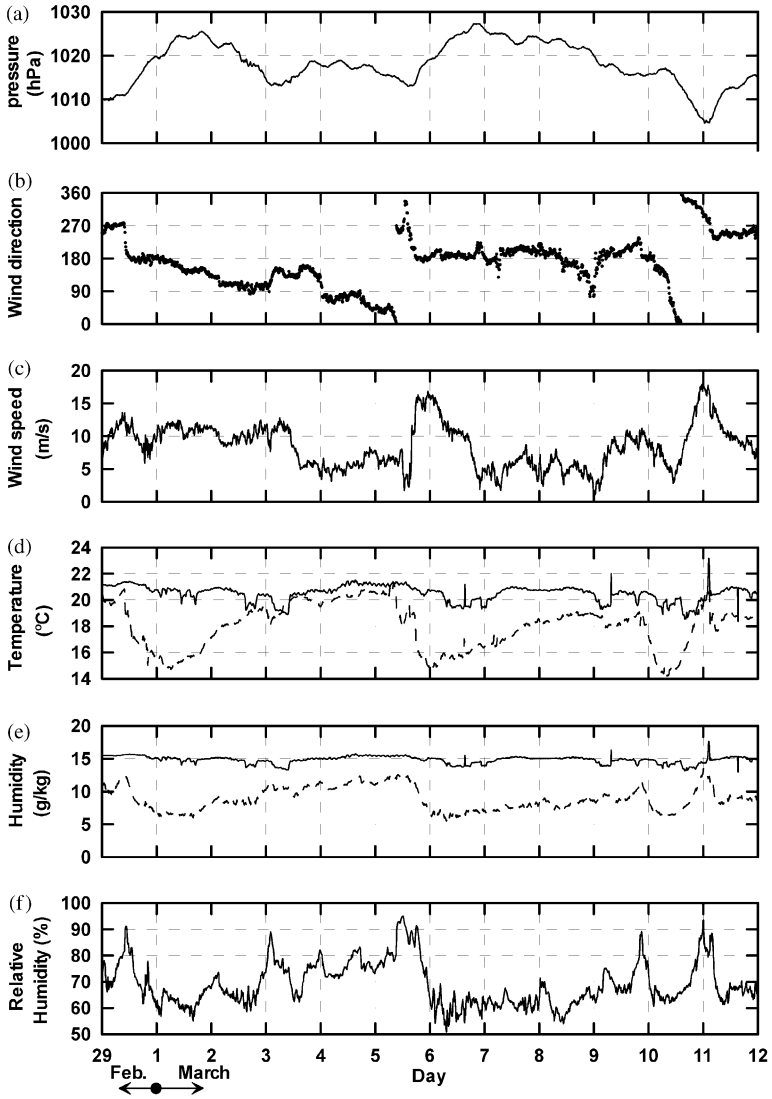

Fig. 15. Time series of the mean parameters required for establishing a net air sea heat budget: air pressure (a), wind direction (b), wind speed (c), temperature (sea-surface—solid and air—dashed) (d), saturation specific humidity (solid) and specific humidity (dashed) (e), and relative humidity (f). The time runs from 29 February to 12 March 2000.

variations of the net heat loss from the sea surface correspond with strong variations of the atmospheric forcing and resulting variations of the turbulent fluxes, especially the latent heat flux (Fig. 16). During sunny conditions (prevailing high pressure system) the latent heat flux reaches extremely high values because of the advection of cold, dry air from the south (compare Figs. 15 and 16). For example, on March 1 the air pressure was high, the prevailing wind was southerly at approximately 10 m/s, and there was a low specific humidity of about 6 g/kg. Table 2 shows the resulting mean heat flux components for that day. The magnitudes of most heat flux components nearly equal the overall mean values in Table 1, but for the turbulent fluxes of sensible and especially latent heat. The sum of the turbulent heat losses on March 1 is 182 W/m^2 larger than

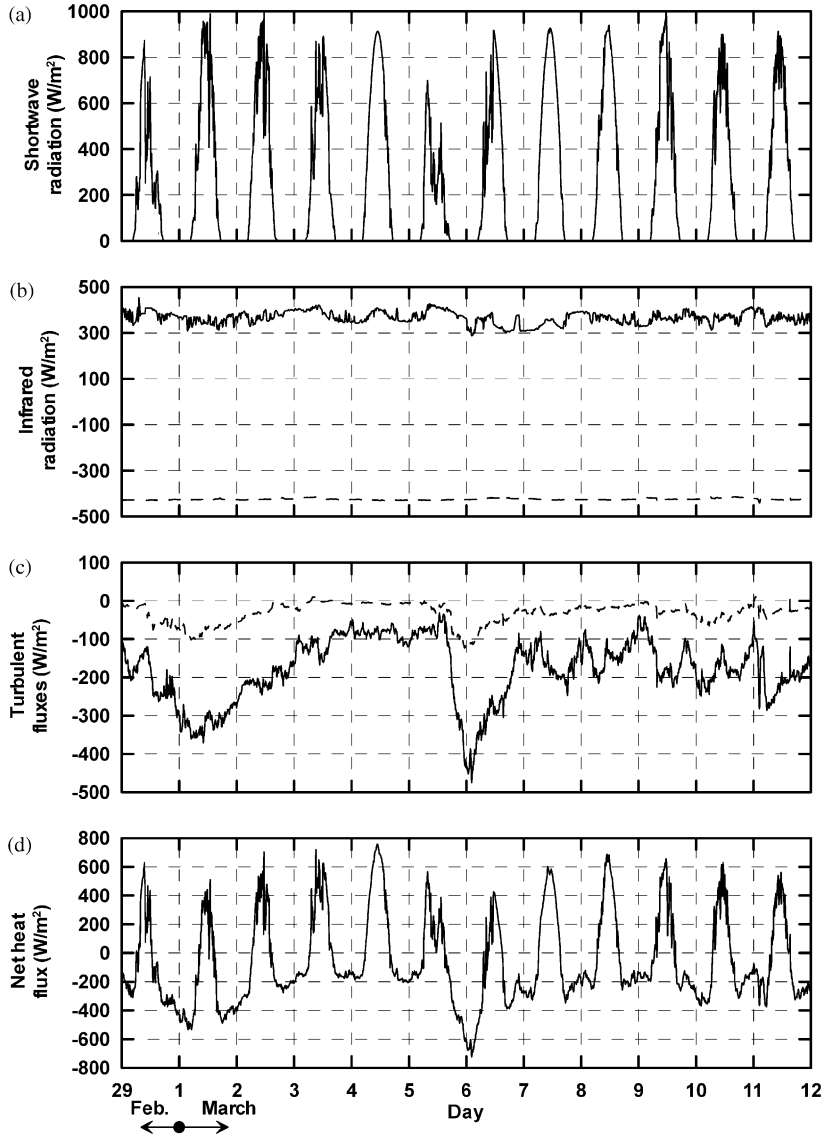

Fig. 16. Same as Fig. 15 for: short wave radiation (a), infrared radiation (incoming—solid and outgoing—dashed) (b), turbulent fluxes (latent heat–solid and sensible heat—dashed) (c) and the net heat flux (d). Positive values indicate heat gain by the sea-surface.

the overall mean and about equals the connected difference of the net heat loss of 179 W/m^2. Similar conditions were encountered on March 6. This illustrates the important contribution of the varying atmospheric forcing for the heat loss of the surface waters in this part of the South Atlantic Ocean in the austral summer. A similar conclusion was drawn by Mey et al. (1990) for a larger area southwest of South Africa.

7. Discussion

7.1. Comparison of central water in Agulhas rings

In order to characterize ring Astrid as a 'typical' or 'atypical' Agulhas ring, a comparison is made with other published ring observations. Such a characterization may be important as the ambition of the MARE programme is to assimilate the

Table 1
Parameters, used for the determination of the sea-surface heat budget (positive = heat gain by the sea-surface) from 29 February to 11 March 2000

Variable	Mean	S.D.	Minimum	Maximum
Air pressure (mbar)	1018	5	1005	1027
Wind speed (m/s)	8.5	3.3	1.0	19.2
SST (°C)	20.5	0.6	18.4	23.2
Air temperature (°C)	18.0	1.7	14.2	21.4
Specific humidity (g/kg)	8.9	1.8	5.5	13.5
Sea-surface specific humidity (g/kg)	14.9	0.6	13.0	17.6
Relative humidity (%)	69.1	8.4	50.9	95.0
Wind stress (N/m^2)	0.15	0.12	0.00	0.78
Atmospheric stability	−0.9	1.5	−19.7	0.0
Latent heat flux (W/m^2)	−180	83	−474	−31
Sensible heat flux (W/m^2)	−32	27	−123	13
Visible radiation (W/m^2)	233	311	0	1065
Outgoing infrared (W/m^2)	−424	4	−439	−412
Incoming infrared (W/m^2)	366	27	288	453
Net heat budget (W/m^2)	−54	312	−724	758

The reflected visible radiation has been omitted from the table. It was calculated as a fixed percentage (7%) of the incoming visible radiation.

Table 2
Daily mean values of the components of the sea-surface heat budget (positive = heat gain by the sea-surface) for March 1, 2000

Variable	Mean
Latent heat flux (W/m^2)	−316
Sensible heat flux (W/m^2)	−78
Visible radiation (W/m^2)	250
Outgoing infrared (W/m^2)	−424
Incoming infrared (W/m^2)	353
Net heat budget (W/m^2)	−233

observed evolution of this ring in a detailed regional model, tune several process parameters, and upscale the results using the altimetry observations of a large ensemble of rings. The rings chosen for comparison were surveyed at about the same location and were either spawned in the same season, or taken as good examples of modification of rings during their life span.

According to Gordon et al. (1987), South Indian Ocean Central Water (SICW) occupies the thermocline in the central part of the Agulhas Retroflection, with an STMW pycnostad at $\Theta \approx 17^{\circ}C$ to $18^{\circ}C$ and $S \approx 35.55$, with a thickness of 130 m. Olson and Evans (1986) and Gordon et al. (1987) described a very young Retroflection Eddy (RE) which also contained this STMW pycnostad. The mixed-layer depth in this ring reaches to over 100 m, with $\Theta \approx 19^{\circ}C$. In the centre of RE the distance between the $17^{\circ}C$ and $18^{\circ}C$ isotherms was about 125 m, definitely larger than the distance between these isotherms observed in Astrid (≈ 50 m). However, in Astrid the STMW pycnostad was centred around the $18^{\circ}C$ isotherm (Fig. 10b), with a distance between the $17.5^{\circ}C$ and $18.5^{\circ}C$ isotherms of about 90 m. In the winter season newly formed rings may rapidly lose heat due to air–sea interaction with the cool South Atlantic atmosphere (Duncombe Rae, 1991). The resulting net cooling rate and deep convection in this area are expected to be much larger in winter than we observed in our summer survey, and may reach a typical seasonal mean value of about 200 W/m^2 (van Ballegooyen et al., 1994). In the older Cape Town Eddy (CTE), also reported by Gordon et al. (1987), the SICW, including the STMW pycnostad, have been eroded completely to 300 m, and cooled to $\sim 16^{\circ}C$ during the preceding winter. The loss of heat due to air–sea interaction will diminish the impact of the rings on the South Atlantic heat budget. We will use the STMW layer as a reference to observe to what extent the Agulhas rings have been modified by winter convection.

Arhan et al. (1999) gave examples of the variety of Agulhas ring properties. They found the STMW pycnostad in one (R2) of their three most distinguished rings (R1, R2, and R3). Although R2 was generated 2 years before the survey and had crossed the Walvis Ridge, it still contained an STMW pycnostad. After formation this ring moved quickly to lower latitudes, and never experienced deep convective cooling in winter. Ring R3 was split from the same initial disturbance as R2, but its main pycnostad was found at $\Theta \approx 13$–14°C, since it was blocked for several months just after spawning. As a consequence R3 was exposed to winter cooling at higher latitudes. In ring R1 the main pycnostad was found at $\Theta \approx 11$–12°C, since it followed an extremely southern course after its formation (to 44°S) where it was exposed to strong winter cooling.

van Ballegooyen et al. (1994) described the properties of four rings, A3–A6. Ring A4 was observed in February–March 1987 at the same latitude as Astrid, but 250 km farther west. This ring was surveyed during the SCARC cruise of R.V. *Agulhas*. Similar to Astrid this ring was apparently formed in the preceding January, but at a latitude of about 41°S, southwest of the retroflection. A4 displayed a thick homogeneous surface mixed layer of about 140 m, with $\Theta = 18.8^{\circ}$C and $S = 35.7$. The relatively low sea-surface temperature in A4 was ascribed to an unrealistic high net heat loss (≈ 420 W/m^2), a value definitely surpassing the fluxes observed during the MARE-1 cruise, and five–six times the summer climatological mean for the area. However, Mey et al. (1990) estimated the mean net heat loss during the SCARC cruise from meteorological observations to be 107 W/m^2. Probably the assumptions made by van Ballegooyen et al. (1994) with regard to the age of the ring, the initial temperature profile or the connected sea-surface temperature were faulty.

Rings RE and A4 were both generated in the same season as Astrid: early austral summer. All three rings were surveyed within 2 months after spawning, and these rings were found in a limited geographic area, 38°–39°S, 15°–18°W. Nevertheless, they differed in hydrographic structure. While the mixed-layer temperatures of RE and A4 hardly differed, they were about 2°C colder than in Astrid. In contrast the mixed-layer depth in A4 was 40–50% larger than in RE and Astrid. While the very young RE showed a thick STMW layer (125 m) this layer was thinner in Astrid (90 m) and A4 (75 m). Moreover, the potential temperature of the STMW core in Astrid was 0.5°C warmer than in RE. The net sea-surface heat flux during the SCARC cruise was definitely larger than the summer climatological mean (-70 W/m^2), while the net heat flux during the MARE-1 cruise was 30% below that of the mean. The differences in these rings, close to their spawning area, suggest that variability of the Agulhas current properties (Lutjeharms, 1996), in combination with varying atmospheric forcing, determine the varying properties of young Agulhas rings close to their spawning area. Comparison with rings R1, R2 and R3 shows that variations in air–sea interaction due to a combination of drift path and season strongly determine the further development of Agulhas rings. The heat and salt content of an Agulhas ring depend to a great extent on the age of the ring, on the modification during convective cooling in different seasons, and on the hydrographic properties of its source, the Agulhas Retroflection, at the time of ring formation. Given these results it seems that Astrid was not an 'atypical' Agulhas ring, but the question arises whether a 'typical' Agulhas ring does exist.

7.2. Characteristic ring parameters

For comparison of Astrid with other Agulhas rings, we also can use characteristic ring parameters, like those defined by e.g., Joyce et al. (1981); Olson and Evans (1986); McDonagh et al. (1999); Garzoli et al. (1999). In part these can be derived directly, in part they are derived from an approximation of the ring in a two-layer diagnostic ring model (McDonagh et al., 1999). The two-layer model approximates the ring structure as a circular symmetric ring with layers of different density. The interface between the layers follows a single isotherm that represents the thermocline within the ring. The model assumes that the lower layer of the fluid is at rest. Our LADCP observations have shown that the rotating velocity field in Astrid extends well to the bottom because of a

Table 3
Integral ring parameters for different Agulhas rings

Source	Programme	Ring	V_{max}[a] (m/s)	L_{max}[b] (km)	Vol_{10}[c] (10^{12} m^3)	APE[d] (10^{15} J)	KE[e] (10^{15} J)	AHA[f] (10^{20} J)	ASA[g] (10^{12}kg)
This study	MARE-1	Astrid	1.0	120	38	20	18	0.8	4.1
van Ballegooyen et al. (1994)	SCARC	A3		160	34			1.5	8.7
		A4		140	33			2.4	13.1
		A5		95	11			0.7	4.4
		A6		125	17			1.1	4.6
Olson and Evans (1986)	ARC	RE	0.9	130	26	51	9		
		CTE	0.6	115	30	31	6		
Duncombe Rae et al. (1996)	BEST	B1-1	0.4	85		17	2	0.2	1.2
	1992–1994	B2-2	0.5	65	17	11	2	0.6	3.8
		B2-3	0.3	85		7	1	0.6	3.7
		B2-4	0.3	95		23	2	0.4	1.7
McDonagh et al. (1999)	A11	Ring 1	0.6	71	15	5	1	0.4	2.4
		Ring 2	0.8	75	24	8	3	0.2	1.4
Garzoli et al. (1999)	KAPEX	Ring 1	0.4	100	31	43	1	0.9	
	1997	Ring 2	0.2	110	42	52		1.3	
		Ring 3	0.3	100	19	15		0.8	

[a] V_{max} is the maximum tangential velocity derived from the gradient balance relation.
[b] L_{max} is the radius where the maximum tangential velocity is found.
[c] Vol_{10} is the volume of the ring above the 10°C isotherm.
[d] APE is the available potential energy relative to the thermocline depth outside the ring.
[e] KE is the kinetic energy of the two-layer ring.
[f] AHA is the integrated heat excess above the 10°C isotherm, relative to a temperature profile which is representative for the surrounding water.
[g] ASA is the integrated salinity excess above the 10°C isotherm, relative to a salinity profile which is representative for the surrounding water.
The parameters L_{max}, Vol_{10}, APE and KE have been derived with a two layer circular symmetric ring model where the thermocline follows the 10°C isotherm. For the determination of AHA and ASA the actual temperature and salinity profiles have been used.

considerable barotropic flow. So the integral ring parameters, derived with this model, mainly present the baroclinic part of the ring. In the Agulhas region the 10°C isotherm is most often used as an approximation for the thermocline, since it usually gives the best correlation with the dynamic height (van Ballegooyen et al., 1994). We also will follow this convention. We will use (Table 3) the following parameters, in agreement with McDonagh et al. (1999): (1) The maximum tangential velocity (V_{max}), derived from the gradient balance relation. (2) The radius (L_{max}) where the maximum tangential velocity is found. (3) The available potential energy (APE) relative to stratification (here thermocline depth) outside the ring. (4) The kinetic energy (KE) of the two-layer ring. (5) The volume of the ring above the 10°C isotherm (Vol_{10}). (6) The available heat anomaly (AHA), which represents the excess heat in the ring above the 10°C isotherm relative to its surrounding water. (7) The available salt anomaly (ASA), which is a measure for the salt excess in the ring above the 10°C isotherm. For the determination of APE, KE, Vol_{10}, AHA and ASA, integration to a boundary radius where the thermocline depth relaxes to the surrounding value is required. For Astrid we have used a radius of 140 km.

Table 3 indicates that V_{max} in Astrid is more than twice the typical maximum tangential velocity reported for other Agulhas rings, observed at a radius L_{max} which is 20% larger than the typical reported size for Agulhas rings. No significant correlation can be established between L_{max} and V_{max}, probably because the ensemble of rings represents rings from different ages and size classes which are not necessarily correlated. The characteristic volume of Astrid, Vol_{10}, is about 50% larger than the mean value for other rings

(25×10^{12} m^3). This can be ascribed nearly completely to the 20% larger radius, indicating that the thermocline depth in Astrid does not deviate significantly from the other rings. While the APE is close to the mean value for the other reported rings, the KE is extremely high, about 6–7 times the typical value for the other rings (2.5×10^{15} J). This can be ascribed nearly completely to twice larger velocities and a 50% larger volume of Astrid, compared with the typical 'average' rings. The available heat and salt anomalies of Astrid are of the same order as the typical values derived for the other rings. So the most significant difference with other rings is the relatively large kinetic energy. The second ring in order of KE is the RE, reported by Olson and Evans (1986) and by Gordon et al. (1987). As already stated above, this ring also is considered to be very young. Since the values of AHA and ASA in Astrid are in the mid-range of the reported rings, while the KE is an order of magnitude larger than in other rings, probably the kinetic energy of Agulhas rings decays faster than their excess heat and salinity content. Unfortunately no V_{max} or KE has been reported for ring A4, which is also very young. Schouten et al. (2000) reported, from an analysis of satellite altimetry data, that the main dynamic decay of Agulhas rings occurs in the first half year of their existence. A delay of heat exchange with their surroundings, compared to the dynamic decay of Agulhas rings, may influence the region where most of the excess heat and salt from Agulhas rings is transferred to the surrounding water. This, in its turn, may directly affect the effectiveness of the Agulhas leakage for the thermohaline circulation. However, we have to recognise that this speculative conclusion is based on a limited number of (sometimes incompletely) reported Agulhas rings.

7.3. Water trapped inside Agulhas rings

From the LADCP velocity profiles it appears that Agulhas rings have a strong barotropic velocity component (Fig. 12). The usual assumption in literature of a level of no motion at 2000 m or even at shallower depths (Olson and Evans, 1986); van Ballegooyen et al., 1994; McDonagh et al., 1999, Duncombe Rae et al., 1996) is proven to be inaccurate for Astrid since a velocity of the order of 10 cm/s is still observed even at 4000 m. This may have considerable consequences for the amount of water trapped inside a ring, since theoretical results suggest that this depends on the ratio of its drift velocity and its tangential velocity (Flierl, 1981). It is, however, questionable whether the results from Astrid can be generalized for all rings. The three rings presented by Garzoli et al. (1999, see also Table 3) all show a different vertical velocity structure. While their ring 3 has a level of no motion near 1000 m, both other rings have still finite velocities of a few cm/s at the maximum observational depth of 1950 m.

In January 2000 ring Astrid was shed from the Agulhas retroflection near 38°S, 17°30′E. From there it drifted within 1 month to a position of about 37°30′S, 18°E, the region where it was still present during the MARE-1 survey. The maximum drift velocity of the ring between January and the end of February, before the MARE-1 cruise, was approximately 3.4 cm/s. In order to trap a considerable part of its water mass during the ring's drift, it seems required that the maximum tangential velocity of the ring, V_{max}, is well above the drift velocity of the ring, V_d. With a ratio $V_{max}/V_d = 4$, over half of the volume of the water in the ring will be trapped and move along with the ring (Flierl, 1981). The typical maximum tangential velocity in the 12°C isotherm, encountered in March 2000, is 75 cm/s, decreasing to 35 cm/s in the 4°C isotherm ($\sim$1000 m) and to about 15 cm/s at the 3°C isotherm (Fig. 11b). So in the first month after formation the tangential velocity above the 12°C isotherm was so large that probably a large part of the warm SICW has been trapped in the ring. At the depth of the intermediate waters ($\sim$1000 m) the tangential velocity was 10 times the drift velocity, enabling the ring to trap most of the original contents of the intermediate water types. It is, however, not clear whether the intermediate and deep waters followed the ring when it was shed from the retroflection, nor during the preceding fast westward translation of the retroflection, since the results from (Flierl, 1981) only apply to ideal circular rings.

7.4. The role of topography

Topography appears to play an important role in the drift and evolution of deep-reaching Agulhas rings (Byrne et al., 1995; Beismann et al., 1999; Schouten et al., 2000). In their early stage mainly the Agulhas Ridge will be responsible for splitting, blocking or changing drift directions of the Agulhas rings Arhan et al. (1999). Due to this blocking effect of the Agulhas Ridge some rings decay already close to the Agulhas Retroflection. According to Arhan et al. (1999), the structures that enter the South Atlantic through the passage between the Agulhas Ridge and the South African continental slope appear to be larger and more energetic than those drifting south of the Agulhas Ridge after their separation.

The possible influence of bottom topography on Agulhas rings has been studied by Kamenkovich et al. (1996), who performed a number of numerical experiments with a two-layer primitive equation model. These experiments mainly dealt with the influence of the Walvis Ridge, but we may extend their conclusions to the Agulhas Ridge. Their primary conclusion was that rings with significant initial vertical shear can cross a Ridge, but barotropic, or near-barotropic rings cannot. Another conclusion was that rings crossing the ridge become more baroclinic compared to their initial state. Our LADCP measurements have revealed that ring Astrid had a strong barotropic component, apparently interacting with the Agulhas Ridge and the continental slope. From satellite altimetry images it has appeared that ring Astrid was indeed moving very slowly for about 6 months before it continued in a northwesterly direction. A year after the MARE-1 survey, ring Astrid had moved not further than 36°S and 12°E. As a result, ring Astrid has stayed at high latitudes during its first austral winter and will have been strongly modified by winter convection.

7.5. Ring–ring interaction

An analysis of the SSH anomalies reveals that the Agulhas Basin and Cape Basin usually have a high density ring population. Consequently these rings strongly interact resulting in splitting and merging (Arhan et al., 1999; Boebel et al., 2003). Arhan et al. (1999) already called this region appropriately the Agulhas Retroflection Cauldron. To what extent these ring–ring interactions influence or dominate the mixing of Agulhas ring water into the surrounding waters still has to be established.

Next to the anti-cyclonic Agulhas rings, also cyclones, with a negative SSH anomaly (Fig. 2, indicated with dashed lines) are observed within the Cape Basin. The influence of these cyclones on the mixing characteristics is also still unknown. Recent studies suggest that a portion of these cyclones also originates in the southwest Indian Ocean (Penven et al., 2001; Lutjeharms et al., 2003). In future Agulhas ring studies, more attention should be given to the interaction of Agulhas rings with other cyclonic and anti-cyclonic structures.

8. Summary and conclusions

During the MARE-1 cruise, in March 2000, the anti-cyclonic Agulhas ring Astrid was observed. This ring was spawned from the Agulhas Retroflection in January 2000 had a maximum SSH anomaly of +70 cm and can therefore be classified as a strong Agulhas ring. Ring Astrid had a radius of 120 km and a volume of $\approx 38 \times 10^{12}$ m^3, which is about 50% larger than the mean value. Together with a large $V_{max}(= 1$ m/s), this results in a large kinetic energy of 18×10^{15} J, which is 6–7 times the typical value. This seems characteristic for young Agulhas rings and probably the kinetic energy of Agulhas rings decays faster than their excess heat and salinity content. The latter two properties are well within the range of other Agulhas rings, reported in literature.

The CTD and LADCP results show that the hydrographic structure as well as the velocity structure of ring Astrid extend down to the bottom, at a depth of over 4500 m, with a large barotropic component. As a consequence, the behaviour of ring Astrid may be influenced by topography like the Agulhas Ridge. The observed translation speed of ring Astrid is low compared to the tangential velocity and it is therefore assumed

that to a large extent water is trapped inside the ring. The water masses within ring Astrid are similar to those found in other rings. Its hydrographic properties differ from those of the surrounding water only at temperatures above 12°C. A minimum in large-scale potential vorticity shows a small layer of Mode Water at $\Theta \approx 18^{\circ}C$, which indicates that there is STMW present. The amount of STMW in ring Astrid is less than in other young Agulhas rings like RE, but more than in A4. This difference can be ascribed to the variability of the Agulhas Current properties and varying atmospheric conditions during the formation of STMW. In the intermediate water layers remnants of RSW are found together with AAIW, similar as in the surrounding water. The observed fine-structure near the ring's boundary suggests that exchange of water with its surroundings already had started.

Even during summer Astrid looses heat ($54\ W/m^2$) to the atmosphere, mainly due to the large mean turbulent flux of latent heat ($-180\ W/m^2$). This heat loss drives the convective mixing in the 90 m thick mixed layer which is observed to be very homogeneous. No systematic difference in heat loss is observed between the ring and its surroundings. This indicates that the atmospheric forcing is the most important factor in determining the net heat budget. Especially periods with advection of cold dry air from the south contribute to a large heat loss to the atmosphere. However, due to the thicker mixed layer in the ring, the sea-surface temperature difference between the ring and its surroundings will be maintained. Nevertheless, the heat loss of recently spawned rings will influence their contribution to the inter-ocean heat exchange of the MOC, and should be accounted for explicitly when the magnitude of the exchange is estimated. Analysis of the modification of Astrid between the successive surveys during MARE, 6 months apart, will shed more light on this subject.

Acknowledgements

We thank captain and crew of R.V. *Pelagia* for their kind co-operation during the MARE-1 cruise. The expertise of technicians and analysts who operated the instrumentation skilfully during the cruise is acknowledged. This research was funded by the Foundation for Earth and Live Sciences (ALW) a subsidiary of the Netherlands Foundation for Scientific Research (NWO) as part of the CLIVARNET programme, under contract number 750.710.01. This is NIOZ publication nr. 3662.

References

Arhan, M., Mercier, H., Lutjeharms, J.R.E., 1999. The disparate evolution of three Agulhas rings in the South Atlantic Ocean. Journal of Geophysical Research 104 (C9), 20,987–21,005.

Beal, L.M., Field, A., Gordon, A.L., 2000. Spreading of Red Sea overflow waters in the Indian Ocean. Journal of Geophysical Research 105, 8549–8564.

Beismann, J.O., Käse, R.H., Lutjeharms, J.R.E., 1999. On the influence of submarine ridges on translation and stability of Agulhas rings. Journal of Geophysical Research 104 (C4), 7897–7906.

Boebel, O., Lutjeharms, J.R.E., Rossby, H.T., Zenk, W., 2003. The Cape Cauldron: an Agulhas mixing and exchange regime. Deep-Sea Research II, this issue (PII: S0967-0645(02)00379-X).

Byrne, D.A., Gordon, A.L., Haxby, W.F., 1995. Agulhas Eddies: a synoptic view using Geosat ERM data. Journal of Physical Oceanography 25, 902–917.

De Ruijter, W.P.M., 1982. Asymptotic analysis of the Agulhas and Brazil Current systems. Journal of Physical Oceanography 12, 361–373.

De Ruijter, W.P.M., Biastoch, A., Drijfhout, S.S., Lutjeharms, J.R.E., Matano, R.P., Pichevin, T., van Leeuwen, P.J., Weijer, W., 1999. Indian–Atlantic interocean exchange: dynamics, estimation and impact. Journal of Geophysical Research 104 (C9), 20,885–20,910.

Duncombe Rae, C.M., 1991. Agulhas retroflection rings in the South Atlantic Ocean: an overview. South African Journal of Marine Sciences 11, 327–344.

Duncombe Rae, C.M., Garzoli, S.L., Gordon, A.L., 1996. The eddy field of the southeast Atlantic Ocean: a statistical census from the Benguela Sources and Transports Project. Journal of Geophysical Research 101 (C5), 11,949–11,964.

Fairall, C.W., Bradley, E.F., Rogers, D.P., Edson, J.B., Young, G.S., 1996. Bulk parametrization of air–sea fluxes for TOGA COARE. Journal of Geophysical Research 101, 3747–3754.

Fine, R.A., 1993. Circulation of Antarctic Intermediate Water in the South Indian Ocean. Deep-Sea Research 40, 2021–2042.

Fine, R.A., Warner, M.J., Weiss, R.F., 1988. Water mass modification at the Agulhas Retroflection: chlorofluoromethane studies. Deep-Sea Research I 35, 311–332.

Flierl, G.R., 1981. Particle motions in large-amplitude wave fields. Geophysical Astrophysical Fluid Dynamics 18, 39–74.

Garzoli, S.L., Richardson, P.L., Duncombe-Rae, C.M., Fratantoni, D.M., Goni, G.J., Roubicek, A.J., 1999. Three Agulhas rings observed during the Benguela Current Experiment. Journal of Geophysical Research 104 (C9), 20,971–20,985.

Goni, G.J., Garzoli, S.L., Roubicek, A.J., Olson, D.B., Brown, O.B., 1997. Agulhas ring dynamics from TOPEX/POSEIDON satellite altimeter data. Journal of Marine Research 55, 861–883.

Gordon, A.L., 1985. Indian–Atlantic transfer of thermocline water at the Agulhas Retroflection. Science 227, 1030–1033.

Gordon, A.L., 1986. Interocean exchange of thermocline water. Journal of Geophysical Research 91 (C4), 5037–5046.

Gordon, A.L., 2001. Interocean exchange. In: Siedler, G., Church, J., Gould, J. (Eds.), Ocean Circulation and Climate. Academic Press, New York, pp. 303–314.

Gordon, A.L., Lutjeharms, J.R.E., Gründlingh, M.L., 1987. Stratification and circulation at the Agulhas Retroflection. Deep-Sea Research 34 (4), 565–599.

Gordon, A.L., Weiss Jr., R.F., Smethie Jr., W.M., Warner, M.J., 1992. Thermocline and intermediate water communication between the South Atlantic and Indian Oceans. Journal of Geophysical Research 97 (C5), 7223–7240.

Joyce, T.M., 1984. Velocity and hydrographic structure of a Gulf Stream warm-core ring. Journal of Physical Oceanography 14 (5), 936–947.

Joyce, T.M., Patterson, S.L., Millard, R.C., 1981. Anatomy of a cyclonic ring in the Drake Passage. Deep Sea Research 28 (Part A), 1265–1287.

Kamenkovich, V.M., Leonov, Y.P., Nechaev, D.A., 1996. On the influence of bottom topography on the Agulhas Eddy. Journal of Physical Oceanography 26, 892–912.

Lutjeharms, J.R.E., 1996. The exchange of water between the South Indian and South Atlantic Oceans. In: Wefer, G., Berger, W., Siedler, G. (Eds.), The South Atlantic: Present and Past Circulation. Springer, Berlin, Heidelberg, pp. 125–162.

Lutjeharms, J.R.E., Boebel, O., Rossby, H.T., 2003. Agulhas cyclones. Deep-Sea Research II, this issue (PII: S0967-0645(02)00378-8).

McCartney, M.S., 1982. The subtropical recirculation of mode waters. Journal of Marine Research 40 (Suppl.), 427–464.

McDonagh, E.L., Heywood, K.J., 1999. The origin of an anomalous ring in the Southeast Atlantic. Journal of Physical Oceanography 29, 2050–2064.

McDonagh, E.L., Heywood, K.J., Meredith, M.P., 1999. On the structure, paths, and fluxes associated with Agulhas rings. Journal of Geophysical Research 104 (C9), 21,007–21,020.

Mey, R.D., Walker, N.D., Jury, M.R., 1990. Surface heat flux and marine boundary layer modification in the Agulhas Retroflection region. Journal of Geophysical Research 95, 15,997–16,015.

Olson, D.B., Evans, R.H., 1986. Rings of the Agulhas current. Deep-Sea Research 33 (1), 27–42.

Ou, H.W., De Ruijter, W.P.M., 1986. Separation of an inertial boundary current from a curved coast line. Journal of Geophysical Research 16, 280–289.

Penven, P., Lutjeharms, J.R.E., Marchesiello, P., Roy, C., Weeks, S.J., 2001. Generation of cyclonic eddies by the Agulhas current in the lee of the Agulhas bank. Geophysical Research Letters 28 (6), 1055–1058.

Schmid, C., Boebel, O., Zwenk, W., Lutjeharms, J.R.E., Garzoli, S.L., Richardson, P.L., Barron, C., 2003. Early evolution of an Agulhas Ring. Deep-Sea Research II, this issue (PII: S0967-0645(02)00382-X).

Schouten, M.W., De Ruijter, W.P.M., van Leeuwen, P.J., Lutjeharms, J.R.E., 2000. Translation, decay and splitting of Agulhas rings in the southeastern Atlantic Ocean. Journal of Geophysical Research 105 (C9), 21,913–21,925.

Stramma, L., Lutjeharms, J.R.E., 1997. The flow field of the subtropical gyre of the Indian Ocean. Journal of Geophysical Research 102, 5513–5530.

UNESCO, 1981. Background papers and supporting data on the International Equation of State of Seawater 1980. UNESCO Technical Papers in Marine Science 38, 1–192.

UNESCO, 1985. The International System of Units (SI) in Oceanography. UNESCO Technical Papers in Marine Science 45, 1–124.

van Ballegooyen, R.C., Gründlingh, M.L., Lutjeharms, J.R.E., 1994. Eddy fluxes of heat and salt from the southwest Indian Ocean into the southeast Atlantic Ocean: a case study. Journal of Geophysical Research 99 (C7), 14,053–14,070.

Visbeck, M., 2002. Deep velocity profiling using Lowered Acoustic Doppler Current Profiler: bottom track and inverse solutions. Journal of Atmospheric and Ocean Technology 19, 794–807.

Weijer, W., De Ruijter, W.P.M., Dijkstra, H.A., van Leeuwen, P.J., 1999. Impact of interbasin exchange on the Atlantic Overturning Circulation. Journal of Physical Oceanography 29, 2266–2284.

Weijer, W., De Ruijter, W.P.M., Dijkstra, H.A., 2001. Stability of the Atlantic overturning circulation: competition between Bering Strait freshwater flux and Agulhas heat and salt sources. Journal of Physical Oceanography 31, 2385–2402.